Tectonophysics 693 (2016) 489–506

Contents lists available at ScienceDirect

Tectonophysics

journal homepage: www.elsevier.com/locate/tecto

Along-fault migration of the Mount McKinley restraining bend of the Denali fault defined by late Quaternary fault patterns and seismicity, Denali National Park & Preserve, Alaska

Corey A. Burkett [a], Sean P. Bemis [a,*], Jeff A. Benowitz [b]

[a] Department of Earth and Environmental Sciences, University of Kentucky, Lexington, KY 40506, USA
[b] Geophysical Institute, University of Alaska Fairbanks, Fairbanks, AK 99775, USA

ARTICLE INFO

Article history:
Received 19 March 2015
Received in revised form 6 May 2016
Accepted 9 May 2016
Available online 13 May 2016

Keywords:
Transpressional tectonics
Thrust fault
Denali National Park & Preserve
Restraining bend
Quaternary geology

ABSTRACT

The tallest mountain in North America, Denali (formerly Mount McKinley, 6,190 m), is situated inside an abrupt bend in the right-lateral strike-slip Denali fault. This anomalous topography is clearly associated with the complex geometry of the Denali fault, but how this restraining bend has evolved in conjunction with the regional topography is unknown. To constrain how this bend in the Denali fault is deforming, we document the Quaternary fault-related deformation north of the Denali fault through combined geologic mapping, active fault characterization, and analysis of background seismicity. Our mapping illustrates an east–west change in faulting style where normal faults occur east of the fault bend and thrust faults predominate to the west. The complex and elevated regional seismicity corroborates the style of faulting adjacent to the fault bend and provides additional insight into the change in local stress field in the crust adjacent to the bend. The style of active faulting and seismicity patterns define a deforming zone that accommodates the southwestward migration of this restraining bend. Fault slip rates for the active faults north of the Denali fault, derived from offset glacial outwash surfaces, indicate that the Mount McKinley restraining bend is migrating along the Denali fault at a late Pleistocene/Holocene rate of ~2–6 mm/yr. Ongoing thermochronologic and structural studies of the Mount McKinley restraining bend will extend these constraints on the migration and evolution of the restraining bend deeper in time and to the south of the Denali fault.

1. Introduction

Strike-slip faults are complex structural systems that commonly have geometric complexities resulting in local zones of convergence or divergence. Restraining bends are those complexities that accommodate convergence, forming zones of localized transpression (Cunningham and Mann, 2007). Restraining bends are curvatures along a strike-slip fault that create space problems between fault blocks (Crowell, 1974). This space problem forces shortening and vertical displacement of crustal material to allow for continued lateral fault slip (Legg et al., 2007) and to improve the mechanical efficiency of the strike-slip fault through the creation of new faults (Cooke et al., 2013).

The transpressive nature of a restraining bend can vary between a tectonic regime that partitions slip into pure strike-slip and pure dip-slip faults to a regime dominated by oblique-slip faults. In a global compilation of restraining and releasing bends, Mann (2007) separates restraining bends into 3 types based on simple geometric attributes: transpressional uplifts, sharp restraining bends, and gentle restraining bends (Fig. 1). Transpressional uplifts occur along a generally straight segment of the major strike-slip fault where the block or plate motion is oblique to the master fault, allowing simple and pure shear to occur together (e.g., Little, 1990). Sharp restraining bends typically have a rhomboidal shape and are characterized by localized uplift on reverse and oblique-slip faults. Gentle restraining bends usually have a lazy S or Z shape and are characterized by a broad deformation zone. The most common restraining bend type is the gentle restraining bend and includes some of the largest restraining bends in the world (e.g., the Lebanese restraining bend; Gomez et al., 2007). Despite being one of the most topographically prominent gentle restraining bends, the Mount McKinley restraining bend (MMRB) of the Denali fault in Alaska has been the subject of only limited study (Fig. 2; Fitzgerald et al., 1993, 1995; Plafker et al., 1992).

The long-term evolution of a restraining bend's geometry has direct implications for how crustal material advects through the restraining bend and the resulting exhumation, topographic development, configuration of active faults and seismic hazards. Some restraining bends appear to migrate along the trace of the primary strike-slip fault through time, such as those along dextral faults of the northern San Andreas fault system of California (e.g., Wakabayashi, 2007). These bends in strands of the San Andreas fault system have produced low topography because new stepover structures have formed to accommodate bend

* Corresponding author.
E-mail address: sean.bemis@uky.edu (S.P. Bemis).

http://dx.doi.org/10.1016/j.tecto.2016.05.009
0040-1951/

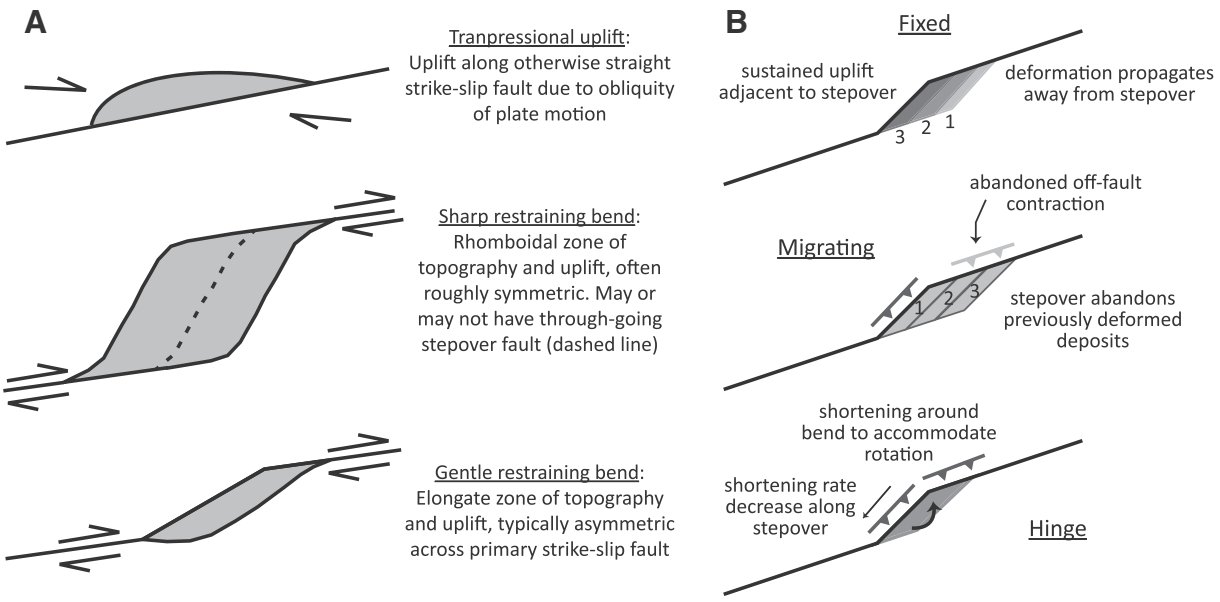

Fig. 1. A) Generalized classification of restraining bends after Mann (2007). Gray regions depict zones of rock uplift and topographic development associated with thrust and/or oblique-slip faults and first-order geometric characteristics are provided for each type. B) Predictions of differences in deformation patterns associated with simple models of gentle restraining bends. The 'fixed' model presumes the stepover fault segment is stable, whereas the 'migrating' model depicts a step-wise abandonment of the existing stepover fault through the creation of new stepover segments. The 'hinge' model depicts a situation where the restraining bend angle increases with time due to rotation of the stepover fault segment. Darker gray denotes regions of sustained rock uplift, and numbers provide a schematic sequence of development with 1 = youngest structures/deformation and 3 = oldest.

migration and do not allow for the continuous uplift of crustal material (Fig. 1; Wakabayashi, 2007). Alternatively, significant topographic highs and regions of focused rock uplift along strike-slip faults, like at the MMRB, are inferred to be associated with restraining bends that are stationary or fixed along the trace of the primary fault, allowing for continuous uplift of crustal material (Fitzgerald et al., 1995; Cunningham and Mann, 2007). Recent wet kaolin modeling calls into question the assumed fixed position of restraining bends relative to topographic highs, and highlights the importance of bend angle in controlling the development of topography and new faults in the

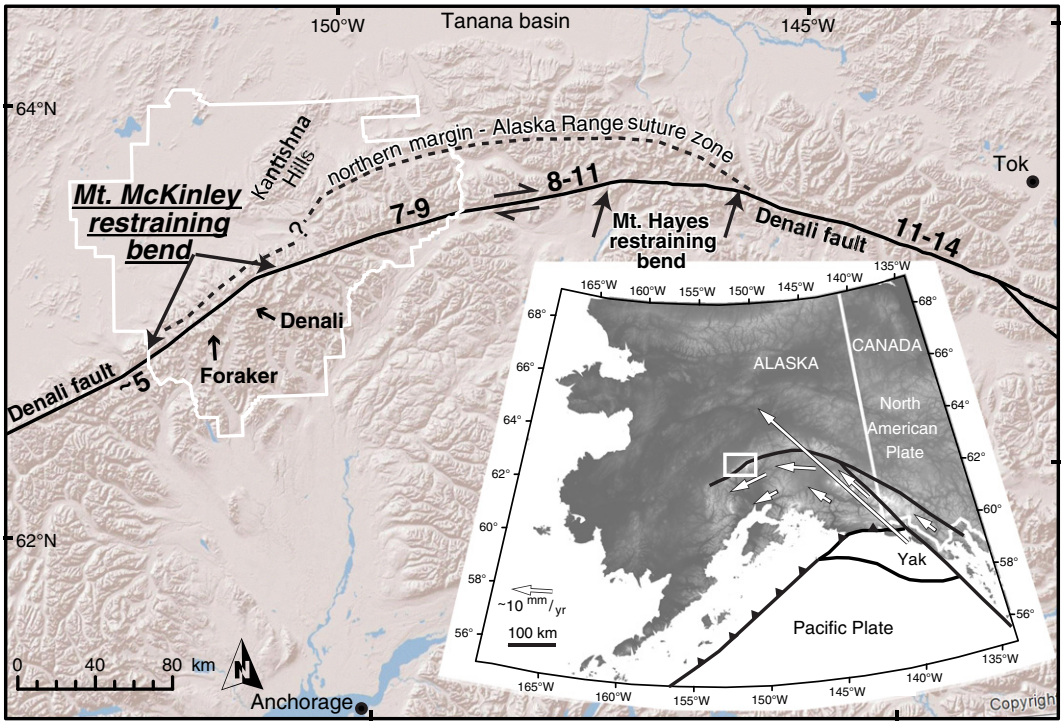

Fig. 2. Regional topography, geographic features, and orogen-scale structures of the Alaska Range–Denali fault system. Numbers along the Denali fault provide approximate late Quaternary slip rates (in mm/yr) derived from Matmon et al. (2006), Mériaux et al. (2009), and Haeussler et al. (2012). The inset map depicts major active tectonic elements for south-central Alaska (modified from Freymueller et al., 2008), showing approximately scaled velocities for the crustal blocks relative to stable North America. The white box on the inset outlines the location of the Mount McKinley restraining bend (MMRB) and the approximate area of Figs. 3 and 4. The white outline is the boundary of Denali National Park & Preserve. The unsubducted portion of the Yakutat microplate is the region in southeast Alaska denoted as 'Yak' on the inset map.

restraining bend (Cooke et al., 2013; Hatem et al., 2015). The relatively simple first-order geometry of the primary strike-slip fault, high rates of vertical tectonics (Fitzgerald et al., 1995), and presence of geomorphic markers that constrain off-fault deformation make the MMRB an excellent natural laboratory for investigations into how a gentle restraining bend evolves.

Observations of spatio-temporal geologic features and deformation patterns, such as rock uplift, fault activity, and fault geometry should allow us to diagnose whether a restraining bend remains fixed or migrates relative to previously deformed deposits. As noted above, fixed restraining bends typically produce significant structural relief adjacent to the stepover fault segment, with the associated rock uplift increasing with greater displacement across the primary strike-slip fault. In contrast, a restraining bend that migrates relative to deformed deposits should produce limited structural relief because the previously deformed crust is abandoned as the focus of deformation progressively acts upon new volumes of crust (e.g. Wakabayashi, 2007; Fig. 1). Deformation can propagate along the primary fault in both settings, but will exhibit different patterns depending upon the migration behavior and the geometry of the fault zone. The primary mode of propagation in a fixed restraining bend should be the widening of the zone of deformation with increasing displacement (e.g., Wakabayashi, 2007; Cooke et al., 2013; Hatem et al., 2015), possibly in the manner of a propagating fold and thrust belt. This widening of the deformation zone will produce along strike propagation of new deformation; however, this propagation would not necessarily occur in conjunction with the abandonment of previously deformed deposits as expected for a migrating restraining bend. Another possible mechanism to produce progressive deformation in a restraining bend is where the angle of the stepover fault segment is increasing relative to the primary strike-slip fault outside of the bend (Fig. 1). The greater obliquity of the transverse fault segment changes the stress field and how slip is partitioned within the deforming zone (Leever et al., 2011). For example, Hatem et al. (2015) use wet kaolin analog models of restraining bends to show that topography develops primarily on one side of the stepover fault where the bend angle is <20° and forms more symmetric across the stepover where the bend angle is >20°. However, it is untested if this topographic asymmetry would persist for a bend that progressively tightened to a bend angle >20°. The key diagnostic feature for a migrating restraining bend is the unidirectional abandonment of previously deformed crust that forms a 'tectonic wake'. Frequently this wake may be expressed by the inversion of progressively younger deposits and by progressively younger low-T thermochronometric cooling ages in the direction of bend migration. Additionally, subsidiary faults that were contractional while they were within the deforming zone may be abandoned or reactivated as extensional structures in the tectonic wake (Fig. 1).

The asymmetric topography across the through-going strike-slip fault of the MMRB results in an abrupt contrast in the development and preservation of Quaternary deposits and geomorphic markers for the study of Quaternary tectonics (Fig. 4). The presence of these deposits and landforms north of the Denali fault provides an avenue to constrain recent deformation rates occurring off the primary strike-slip fault. To accomplish this we conducted regional Quaternary geologic mapping to document the distribution of Quaternary deposits, establish relative age control, and to provide a framework for recognizing active fault traces and geometries. We examine the local seismicity for spatial trends to improve interpretations of subsurface fault geometries. We propose a model for the southwestward migration of the MMRB that integrates the known geometries and slip rates of active faults within and adjacent to the restraining bend.

2. Geologic background

The crust of south-central Alaska was progressively built by the accretion of transported continental fragments and island arcs that collided with the southern Alaska plate margin (e.g., Coney and Jones, 1985; Plafker and Berg, 1994). Sedimentary basins and accretionary complexes record the collision and accretion of these exotic terranes and these are preserved as highly deformed and relatively weak crustal-scale suture zones (Trop and Ridgway, 2007). These crustal-scale weaknesses between accreted terranes act to focus some of the transferred stress from the modern southern Alaska plate boundary to produce long-term, high magnitude displacements within the continental crust (Fitzgerald et al., 2014a). In particular, the Alaska Range suture zone, which represents the Mesozoic collision of the Wrangellia composite terrane with the former North American plate margin (e.g., Ridgway et al., 2002), is occupied by the Alaska Range, a major, active transpressional orogen formed along the intracontinental Denali fault system (Fig. 2). The Denali fault localizes crustal stresses transmitted from the active flat-slab subduction and accretion of the Yakutat microplate along the southern Alaska convergent plate boundary (Fig. 2; Eberhart-Phillips et al., 2006; Ferris et al., 2003; Freymueller et al., 2008; Haeussler, 2008; Worthington et al., 2012) and has helped to drive the growth of the Alaska Range over the past ~25 m.y. (Benowitz et al., 2011, 2012b, 2014; Riccio et al., 2014).

The Alaska Range is the orogenic product of oblique plate motion imposed upon the Denali fault which acts to partially decouple southern Alaska from the North American crust to the north (Bemis et al., 2015a, 2015b; Fitzgerald et al., 2014b; Jadamec et al., 2013). Quaternary deformation in the Alaska Range is primarily slip-partitioned between right-lateral strike-slip and local dip-slip on the Denali fault system (Benowitz et al., 2011), SW-striking thrust faults and Denali fault-parallel thrust faults that lie south of and intersect the Denali fault (Haeussler, 2008; Riccio et al., 2014; Terhune et al., 2015), and Denali fault-parallel thrust faults to the north (Bemis et al., 2015a, 2015b; Bemis et al., 2012; Bemis and Wallace, 2007; Carver et al., 2008, 2010). Along the Denali fault are two prominent gentle restraining bends that create focused zones of deformation, the Mount Hayes restraining bend (Fig. 2; Fitzgerald et al., 2014a, 2014b) and the aforementioned MMRB (Benowitz et al., 2012a; Fitzgerald et al., 1995). In this study we focus on the less studied MMRB.

3. Geologic setting of the MMRB

The MMRB is a gentle restraining bend that consists of a ~75 km-long, through-going fault segment connecting the west-central Denali fault and the western Denali fault (Fig. 3). Both ends of this connecting (stepover) segment form abrupt bends that change strike over a distance of <3 km (Reed and Nelson, 1980; Reed, 1961). We use the term 'vertex' to represent the point of intersection of these fault segments and to act as a geometric marker that is not attached to either side of the fault. Denali occupies the inside of the 18° bend formed at the eastern end of the stepover fault — the 'eastern vertex' of the MMRB. The south side of the Denali fault through the MMRB is dominated by a broad, up to 50 km wide, swath of tall, rugged, glaciated peaks, culminating with Denali (6190 m; Fig. 4). In contrast, the north side of the Denali fault contains only a narrow band of foothills restricted to within 15 km of the fault (the Peters Dome foothills) with Peters Dome a topographically anomalous glaciated high point at 3222 m (Fig. 4). The contrasting morphology across the MMRB indicates structural control on local orogenic development.

The bedrock geology of the Peters Dome foothills consists of polymetamorphosed Precambrian to Paleozoic rocks of the Yukon Tanana terrane, Jurassic, Cretaceous and Tertiary sedimentary rocks, and Paleocene to Eocene volcanics (Fig. 3; Reed, 1961; Wilson et al., 1998). The northern margin of the Alaska Range suture zone, known as the Hines Creek fault in the Alaska Range east of the MMRB (e.g., Brennan et al., 2011; Ridgway et al., 2002, 2007), passes through the Peters Dome foothills subparallel to the Denali fault (Fig. 3). This fault separates the Paleozoic rocks of the former North American plate margin from the Mesozoic accretionary deposits associated with the docking of the Wrangellia terrane (Ridgway et al., 2002). Late Cretaceous sedimentary

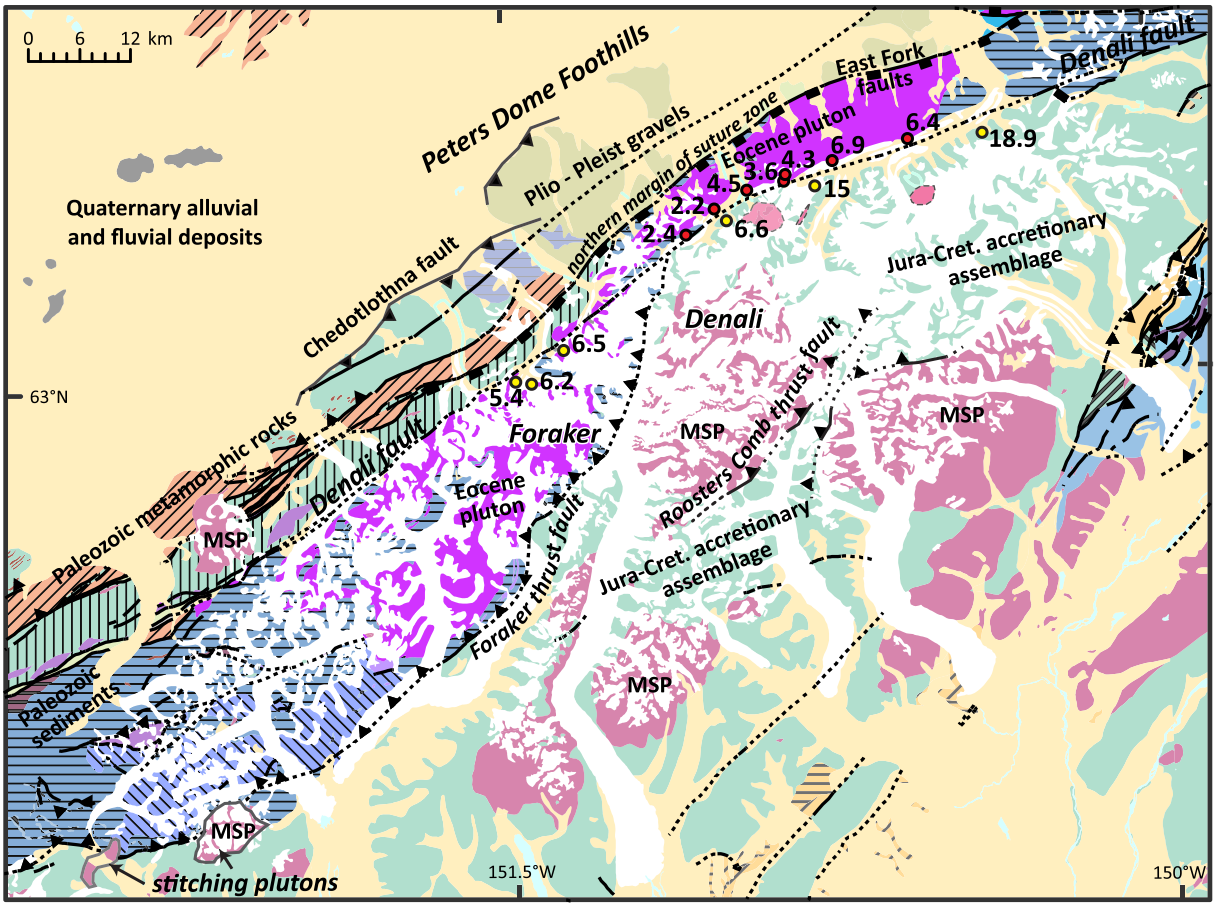

Fig. 3. Generalized geology of the MMRB region with base map modified from Wilson et al. (1998). Fault traces illustrate previously recognized faults from Wilson et al. (1998), Hauessler (2008), and Bemis et al. (2012); additional details on new active fault mapping presented on Fig. 5. Plutons of the McKinley Sequence (MSP; Lanphere and Reed, 1985) and Eocene plutons intrude the complexly deformed accretionary assemblage and translated terranes of the Mesozoic Alaska Range suture zone. The northern margin of this suture zone is shown on the map and appears to be locally reactivated by Quaternary faults. Trends in preliminary apatite fission-track (red dots north of Denali fault) and zircon (U–Th)/He (yellow dots south of Denali fault) cooling ages (in Ma) illustrate a westward migrating focus of deformation.
Data from Terhune et al. (2014) and Bemis et al. (2015a, 2015b).

rocks of the Cantwell Formation represent a basin formed across the Alaska Range suture zone during the waning phases of the associated terrane accretion episode (Ridgway et al., 1997; Salazar-Jaramillo et al., 2016; Tomsich et al., 2014). The Cantwell Formation is unconformably overlain by the Paleogene Teklanika Formation (also known as the Upper Cantwell Formation) which is a sequence of volcanic rocks consisting of andesite and rhyolite with some basalt and pyroclastic rocks (e.g., Gilbert et al., 1976). Collectively, the Cantwell and Teklanika formations constitute the Cantwell basin, which is primarily preserved between the Denali and Hines Creek faults (Csejtey et al., 1992; Reed, 1961). In the Peters Dome foothills, the only mapped geologic units younger than the Teklanika Formation are the Plio-Pleistocene(?) Nenana Gravel and the sequence of Quaternary glacial and surficial deposits.

4. Active tectonics of the MMRB

Despite ~100 years of geological mapping efforts in the region and the known correlation between restraining bends and active deformation (e.g., Mann, 2007), the only faults north of the MMRB identified as active during the Quaternary prior to this study include Peters Dome fault and the East Fork faults (Bemis et al., 2012; Koehler et al., 2012; Plafker et al., 1994).

Recent re-interpretation of regional bedrock mapping and geomorphic observations of incised meanders and warped glacial deposits provide evidence of the broad and gently asymmetric Kantishna Hills anticline (Bemis et al., 2012; Ruppert et al., 2008). This fold has tilted Plio-Pleistocene alluvial deposits on its margins and trends oblique to the Denali fault-parallel thrust faults of the northern Alaska Range thrust system to the east (Fig. 2). Also using the Plio-Pleistocene alluvial gravels as a marker for Quaternary deformation, Bemis et al. (2012) document the Peters Dome fault is a south-dipping thrust fault that defines a portion of the topographic range front of the Peters Dome foothills (Fig. 3). The other faults in the region previously considered as active in the Quaternary, the East Fork faults (Fig. 3; Plafker et al., 1994) are documented as two short fault traces with young geomorphic scarps. The Denali fault is the primary active fault of the MMRB, exhibiting a continuous geomorphic expression through the region. East of the MMRB, the fault trace consists of youthful fault scarps within a broad fault-parallel trough and two studies document late Quaternary slip rates of ~7–9 mm/yr (Fig. 3; Haeussler et al., 2012; Mériaux et al., 2009). Within the MMRB this topographic trough is filled with active glaciers and although the trace is evident where the fault crosses bedrock ridges between glaciers, no direct slip rate measurements exist for this portion of the fault. West of the MMRB the Denali fault trace is not as obvious as to the east, but is apparent in aligned fault parallel valleys with a locally visible fault scarp. Haeussler et al. (2012) document a slip rate of ~5 mm/yr for this portion of the fault (Fig. 2).

The MMRB region exhibits a high level of background seismicity with M2 and larger earthquakes occurring weekly at depths less than 20 km (http://www.aeic.alaska.edu/). While relatively frequent, the majority of historic earthquakes are small (<M3), with the cumulative

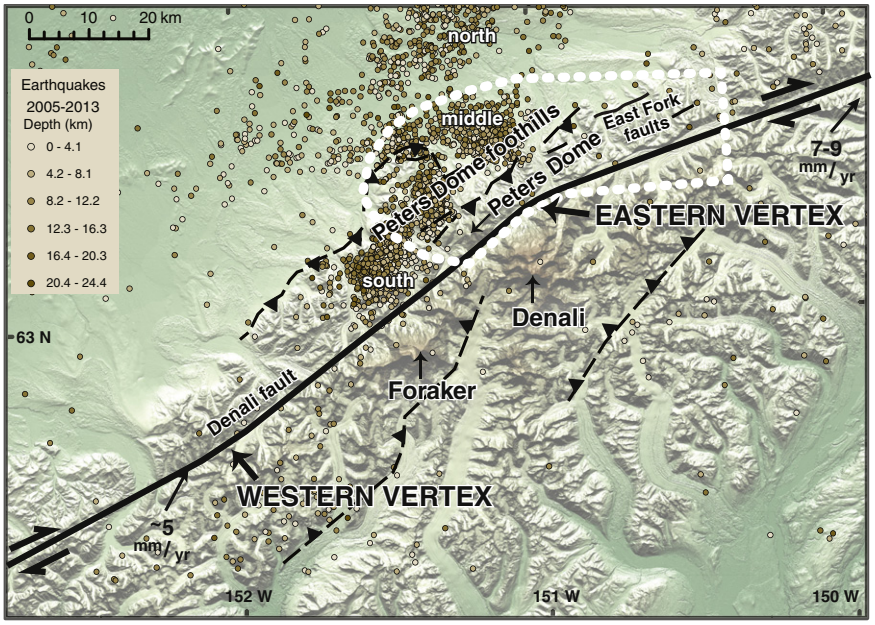

Fig. 4. Active structural features and crustal seismicity of the MMRB. The abrupt bends in the Denali fault that define the endpoints of the stepover fault segment of the MMRB are termed the eastern and western vertexes. The dotted outline illustrates the coverage of the Quaternary geologic map in Fig. 5. Earthquakes shown are a subset from 2005 to 2013 of the full dataset used in this study and shown with a maximum depth of 25 km. Hypocenters are colored by depth with a red gradient indicating increasing depth to a maximum of 25 km. The north, middle, and south refer to subzones of Kantishna cluster seismicity defined by Burris (2007). Slip rate constraints shown for the nearest sites east and west of the MMRB (Mériaux et al., 2009; Haeussler et al., 2012).

seismic moment only equivalent to a M_W5.6 during the time interval of 1990 to 2006 (Burris et al., 2007). Typically referred to as the Kantishna cluster (e.g. Ruppert et al., 2008) this high frequency, clustered seismicity suggests the occurrence of active Quaternary deformation in the Peters Dome foothills (Fig. 4).

Seismologists have noted that despite the abundant shallow crustal seismicity, there are no previously-mapped active faults that correspond with the style and trends of the Kantishna cluster (Burris, 2007). Ruppert et al. (2008) used relocated earthquake hypocenters to conclude that seismicity in the cluster rarely extends deeper than 12 km, providing an approximate seismic limit for the local crust. Initially, Ratchkovski and Hansen (2002) identified two clusters of earthquake hypocenters trending about SW–NE and WNW–ESE that characterized the Kantishna cluster, with the northern section showing mainly reverse/thrust slip and strike-slip focal mechanisms while the southern section showed mainly right lateral strike-slip focal mechanisms. More recent analysis of the Kantishna cluster has led to the subdivision of the local seismicity into 3 subzones, distinguished by clusters of earthquake epicenters within the region (Fig. 4; Ruppert et al., 2008; Burris, 2007). The north and south subzones are oriented parallel to the nearest portion of the Denali fault, whereas the middle zone is oriented oblique to the restraining bend. Earthquake focal mechanisms exhibit primarily strike-slip and reverse/thrust earthquakes (Burris, 2007) and stress tensor inversion of these data illustrate that the stress regime is heterogeneous. Ruppert et al. (2008) notes a consistent rotation of the maximum compressive stress from NNW in the north subzone to WNW in the south subzone (Ratchkovski and Hansen, 2002; Burris, 2007). These zones of deformation appear to highlight the complex crustal response to restraining bend deformation and provide an opportunity for detailed neotectonic studies to identify geologic evidence of potential seismogenic sources. By documenting the style of active faulting north of the eastern vertex of the MMRB, our study provides new context for interpretation of Kantishna cluster seismicity and how it relates to the evolution of the MMRB.

5. Methods

We mapped the surficial geology and neotectonic landforms at 1:24,000 scale covering the Peter Dome foothills across the eastern vertex of the restraining bend to construct a framework for understanding the Quaternary deformation of the MMRB (Fig. 5). The previous mapping was compiled at 1:250,000 scale and conducted largely prior to the publication of the systematic topographic map coverage for the region (Reed, 1961). This map provides a general framework for the regional geology, but does not provide sufficient detail for Quaternary geologic and structural studies. Due to the remote location of the field area and to minimize impact within the Denali National Park & Preserve, most of our surficial mapping coverage was completed remotely. With tree coverage restricted to the lowermost elevations of the field area, surficial deposits are well-defined in IfSAR-derived digital elevation data (~2.5 m cell size; http://ifsar.gina.alaska.edu/) and sub-meter resolution satellite imagery (obtained from the Polar Geospatial Center). This remote mapping was supplemented with low sun-angle oblique photographs collected during fixed-wing overflights (August 2012) of the field area. Fieldwork during summer 2013 allowed us to check preliminarily mapped contacts, complete unit characterization (Table 1), and supplement mapping with field measurements and topographic profiles. For age control on the surficial deposits, we first correlated our mapping with Reed (1961) and Dortch et al. (2010a) to make regional correlations with the regional glacial stratigraphy of the Alaska Range established by Ten Brink and Waythomas (1985), and then we used data reported by Dortch et al. (2010b) to tie the relative chronology to existing age control. We contribute a new direct age on deposits within the map area where we analyzed 5 radiocarbon samples subsampled from a block of a buried soil. These samples were prepared at the University of Kentucky and then sent to Lawrence Livermore National Laboratory Center for Accelerator Mass Spectrometry for pretreatment and analysis.

Based on our mapping, we used deformed or offset Quaternary landforms to define the occurrence of active fault traces, their lateral extent,

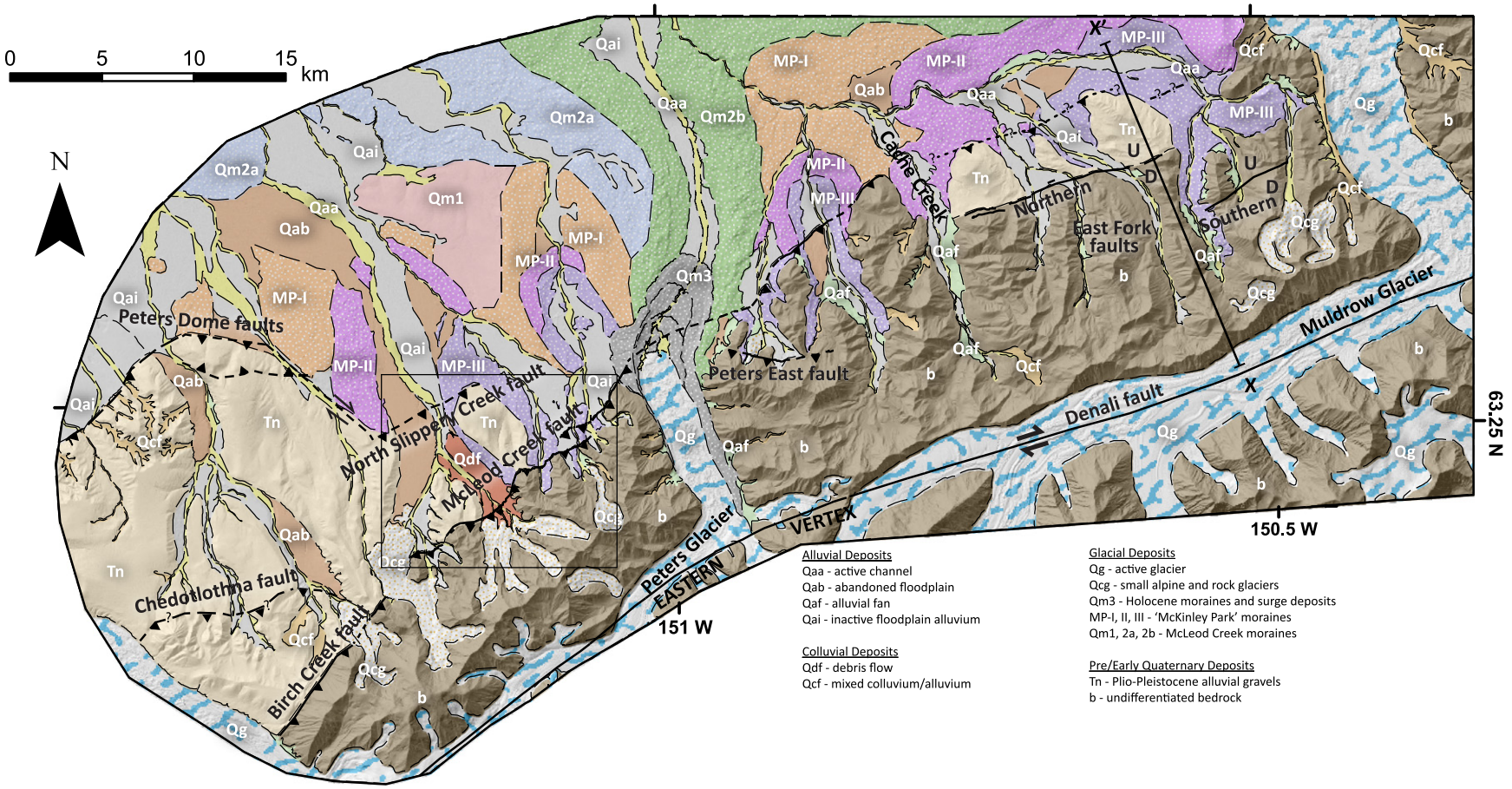

Fig. 5. Quaternary geology of the Peters Dome foothills across the eastern vertex of the MMRB. Unit descriptions provided in text and in Table 1. Inactive faults and unit contacts within bedrock are not shown to emphasize the patterns of Quaternary deformation and unit correlations. Relative motion across the East Fork faults shows the sense of motion defined by the fault scarp, which is opposite of the mapped geologic relationships. The presence of an inactive, buried thrust fault north of the East Fork faults is inferred from the uplift of the Plio-Pleistocene alluvial gravels above lowlands to the north. Note the east-west change in active fault style and orientation across Cache Creek. Map units are shown as partially transparent over shaded relief topography image to illustrate the association of faults and surficial units with topography. Black rectangle shows the region of Fig. 7. X–X′ is the line of section for the schematic cross-section in Fig. 14.

Table 1
Quaternary geologic map unit descriptions.

Unit	Description
Alluvial deposits	
Qaa — active channel	Active channel deposits characterized by boulder-cobble dominated surface, presence of active or ephemeral stream flow, and sparse to no vegetation.
Qai — inactive floodplain alluvium	Fluvial landforms forming small benches along drainages, often with riparian vegetation suggesting occasional inundation during high water. Deposits are well-drained, moderately to poorly sorted cobble-boulder gravel often capped by a thin sand sheet.
Qab — abandoned floodplain	The highest post-glacial fluvial landforms with fully developed tundra or boreal forest vegetation and often display bar and swale topography. Deposits are well-drained, moderately to poorly sorted cobble-boulder gravel.
Qaf — alluvial fan	Characteristically fan-shaped landforms with moderately-sorted cobbly gravel deposits that typically occur along the sides of the larger stream valleys
Colluvial deposits	
Qcf — mixed colluvium/alluvium	Poorly-sorted gravelly deposits occurring along the base of hillslopes and on the valley floors of short, ephemeral drainages
Qdf — debris flow	Sheets of diamict overlying post-glacial floodplains and alluvial fans. Surfaces contains numerous large boulders but do not exhibit morainal topography.
Glacial deposits	
Qg — active glacier	Extent of large active valley glaciers, based on DEMs and imagery spanning 2005–2011
Qcg — small alpine and rock glaciers	Small glaciers and rock glaciers (mixed talus and ice) that occur primarily in the higher, north-facing cirques and valleys in the map area.
Qm3 — Holocene moraines	Moraine and possibly surge deposits from the most recent (Holocene) advances of the Peters and Muldrow glaciers
MP-I–III — McKinley Park moraines	'McKinley Park' moraine sequence are late Pleistocene moraines originally mapped by Ten Brink and Waythomas (1985). Our mapping used morphological and superposition characteristics to extend the distribution of these deposits westward across the map area.
Qm1, 2a, 2b — McLeod Creek moraines	'McLeod Creek' moraine sequence originally mapped by Reed (1961). Qm1 moraines are generally devoid of kettles but exhibit smooth, broadly hummocky surfaces. May be comprised of multiple early and mid-Pleistocene moraine deposits. Qm2a and Qm2b are subdivisions of Qm2 of Reed (1961) and are characterized by abundant kettle ponds and hummocky surfaces.
Pre/early-Quaternary deposits	
Tn — Plio-Pleistocene gravel	Coarse-grained, massive/weakly bedded alluvial cobble-boulder gravel deposit with locally-preserved geomorphic surface defining the top of the unit. Likely correlative to the Nenana Gravel mapped elsewhere in the Alaska Range (e.g., Ridgway et al., 2007), but this deposit displays a lesser degree of lithification than the already weakly lithified Nenana Gravel.
b — undifferentiated bedrock	Composed of a wide range of metamorphosed Precambrian to Paleozoic volcanic and sedimentary rocks, Mesozoic sedimentary rocks, Paleocene-Eocene volcanic rocks, and Eocene felsic intrusive rocks.

* See Table 2 for age and correlation details.

and their sense of displacement. We supplemented the remote mapping with observations of fault dips and topographic surveys across fault scarps. The topographic surveys were performed using a hand-held Trimble 6000 series GPS (decimeter-scale post-processed precision) to define scarp structure and measure the cumulative slip for the offset geomorphic surface. To supplement limited surface constraints on subsurface fault geometry, we examine the abundant shallow crustal seismicity in map-view and cross-section for trends of hypocenters that may define subsurface structures. We incorporate hypocentral data for all earthquakes from 1968 to 2013 as well as available focal mechanism data from the Alaska Earthquake Information Center.

6. Mapping of Quaternary geology

Due to our focus on Quaternary deformation, in our mapping of the Peters Dome foothills region we distinguished, 1) Pre-Neogene bedrock composed of metamorphic, igneous and sedimentary rocks, 2) Plio-Pleistocene alluvial deposits, and 3) Quaternary glacial, alluvial, and colluvial deposits. Despite the proximity to the high, glaciated peaks of the Denali area, portions of our map area outside of the large glacial lobes and alpine glaciers were free of ice during Pleistocene glacial maxima (Figs. 4 and 5). As a result, the Quaternary geologic record extends at least to the mid-Pleistocene with glacial advances that are broadly correlative with major climatic events. General descriptions of the units are provided below, with more complete descriptions provided in Table 1.

6.1. Pre-Neogene bedrock — b

Regional-scale geologic mapping of the Peters Dome foothills (Reed, 1961; Wilson et al., 1998) depicts the bedrock geology of the Peter Dome foothills as consisting of thin, fault-parallel bands of rocks that become progressively older to the north, are locally intruded by plutons and are overlain by volcanic rocks. Our field observations support modifications made in Wilson et al. (1998) from the Reed (1961) unit correlations and provide more precise locations for faults and unit contacts.

6.2. Plio-Pleistocene alluvial deposits — Tn

Exposures and subcrop of massive, poorly sorted, boulder to cobble conglomerates occur across the northern margin of the Peters Dome foothills. The unit is weakly lithified and characteristically forms subdued hills with gravelly ridge crests. This unit also underlies a prominent plateau-like geomorphic surface that appears to be the remnants of an uplifted basin surface. The sedimentology and depositional style of these deposits are similar to the Nenana Gravel, a widespread Miocene-Pleistocene(?) coarse-grained sequence of alluvial fan and braidplain deposits mapped across the northern foothills of the Alaska Range (e.g., Péwé et al., 1966; Ridgway et al., 2007; Wahrhaftig, 1958). These foreland basin gravel deposits contain a stratigraphic record of the growth of the modern Alaska Range (e.g., Ridgway et al., 2007).

6.3. Quaternary deposits

Most of the Quaternary deposits mapped in the Peters Dome foothills are associated with major glacier fluctuations of the mid to late Pleistocene and reflect a similar glacial sequence as is documented elsewhere in the Alaska Range (e.g., Dortch et al., 2010b; Matmon et al., 2010; Wahrhaftig, 1958). The Peter Dome foothills are transected by several large modern glaciers that are sourced in the high peaks south of the Denali fault, whereas numerous cirque and small valley glaciers have smaller accumulation areas and are limited to the north side of the Denali fault (Figs. 4 and 5). Glacier deposits are widespread throughout the foothill valleys and on the lowlands to the north. The extent of glaciers during the last glacial maximum is evident by the glacial moraine deposits that line the valley walls (MP-III), while other moraine deposits (MP-I, MP-II, Qm1, Qm2a, Qm2b) cover the lowlands and plains to the north (regional and marine isotope stage correlations summarized in Table 2). The McKinley Park glacial episodes (MP-I-III) are mapped following Dortch et al. (2010a) and we extend these units through the foothills west of the vertex by mapping morphology and superposition of the moraine deposits. Reed (1961) generally mapped two major sets of Pleistocene glacial moraine deposits (Qm1 and Qm2). However, based upon surface morphology and superposition, we subdivide Qm2 into two separate advances, as well as recognize

Table 2
Age correlations of glacial deposits within the peters dome foothills.

Mapped glacial deposit	Muldrow McKinley Park correlation[b]	Nenana River valley correlation[c]	Delta River correlation[d]	Marine isotope stage correlation	Age range (ka)[e]
Qm3	"X"/"Y" drift			MIS 1	<2
MP-III	MP-III	Carlo Creek (16 ± 1.8 ka)	Donnelly (15-19 ka)	MIS 2	15.1–12.3
MP-II	MP-II	Riley Creek 2/Carlo Creek	Donnelly (15-19 ka)	MIS 2	20.6–19.9
MP-I	MP-I	Riley Creek 1		MIS 2	21.4–20.6
Qm2a	McLeod Creek	Healy		MIS 4	57–71
Qm2b	McLeod Creek	Healy		MIS 4	57–71
Qm1[a]		Browne?		>MIS 6	>191

[a] Our Qm1 corresponds with Qm1 mapped by Reed (1961), although he tentatively correlates Qm1 with the Healy advance of the Nenana River valley sequence. It appears what Reed (1961) maps as Qm1 encompasses multiple older glacial advances based upon superposition of landforms and wide variation in moraine morphology (roughness, presence of kettles) between different moraines.
[b] Correlations based upon the summary by Dortch et al. (2010a).
[c] Correlations based upon Wahrhaftig (1958) and Dortch et al. (2010b).
[d] Correlations based upon Matmon et al. (2010).
[e] Ages derived from Dortch et al. (2010a,b); Briner and Kaufman (2008), and correlations with the global marine isotope stages.

that Qm1 is likely composed of deposits from multiple mid-Pleistocene glacial advances (Tables 1 and 2).

Occupying the space between the bedrock ridges and moraine deposits is a complex of predominantly Holocene alluvial and colluvial deposits (Fig. 5). Almost all moraine deposits have been cut by high-energy streams occupying cobble and boulder dominated channels (Qaa). Along these active streams, floodplains that are abandoned or only occupied at extreme flows are characterized by accumulation of fine-grained sediment, which allows the advancement of the boreal forest vegetation onto these surfaces (Qai, Qab). The transition from the valley floors to the slopes of the bedrock ridges is typically a complex composed of mixed colluvial/alluvial deposits (Qcf) and small alluvial fans (Qaf). Several cirques are occupied by active glaciers or small rock glaciers (Qcg) and these are primarily restricted to moderate elevation north-facing valleys east of the Peters Glacier (Fig. 5).

7. Age control

The north side of the Alaska Range was generally ice-free except for several large valley glacier systems during the Pleistocene glaciations, allowing for moraines from multiple glacial advances to be preserved throughout the Peters Dome foothills with correlative deposits across the range (e.g., Briner and Kaufman, 2008; Ten Brink and Waythomas, 1985; Wahrhaftig, 1958). The last glacial maximum in Alaska corresponds with marine isotope stage (MIS) 2, and of these MIS 2 moraines, the most extensive advance (MP-I) is dated at ~21.4–20.6 ka, with successively younger advances occurring at ~20.6–19.9 ka (MP-II), ~15.1–12.3 ka (MP-III), and ~12.3–11 ka (MP-IV) (Ten Brink and Waythomas, 1985). The oldest alluvial fans and floodplain surfaces up-valley from the MP-II and MP-III moraines must post-date the emplacement of those moraines and likely correlate with MP-IV of Ten Brink and Waythomas (1985) near the Pleistocene–Holocene transition. The relative ages and our correlations of the glacial deposits along the foothills are provided in Table 2.

8. Mapping of Quaternary structures and patterns relative to the MMRB

Recent studies of Quaternary faulting in the Alaska Range have documented numerous previously unknown active faults through the reinterpretation of regional-scale mapping and the recognition of fault scarps and folding of Quaternary landforms and deposits (Bemis and Wallace, 2007; Carver et al., 2008, 2010; Bemis et al., 2012). Through remote mapping of the Peters Dome foothills, we document 5 previously unmapped fault traces (Fig. 5) as well as establish geologic relationships associated with fault scarps referred to by Reed (1961). Many of the active faults in the Peters Dome foothills are well-defined by fault scarps that are relatively continuous across the foothills, offsetting everything but the active channel deposits. Other active faults are defined based on mapped relationships of uplifted and deformed Plio-Pleistocene deposits that constrain the faulting style and simple geometry, even though scarps are not obvious. Nearly all the active faults in the Peters Dome foothills are sub-parallel to the Denali fault; however, there is a clear transition in the sense of displacement from east to west across the eastern vertex of the MMRB.

8.1. East of the eastern vertex

Active faults east of the eastern vertex (east of Peters Glacier) illustrate a rapid shift from S-SE dipping thrust faults near the vertex to south-dipping normal faults east of the bend (Fig. 5). Thrust faults are restricted to the area west of Cache Creek. In the region between Cache Creek and the eastern vertex, the McLeod Creek fault forms a range-bounding thrust fault parallel to the stepover segment of the Denali fault and the Peters East fault occurs parallel to the Denali fault east of the vertex (Fig. 5). The McLeod Creek fault has a clear geomorphic expression where it offsets multiple geomorphic surfaces with offsets of early Holocene(?) floodplain surfaces up to ~15 m, but the trace is not well-expressed across the younger, late Holocene deposits. The trace of the south-dipping Peters East fault lies along the base of a distinct east-west trending ridge, but only exhibits a small fault scarp across the active alluvial fans, talus slopes, and young floodplain surfaces. Evidence for active thrust faulting is absent on the west side of Cache Creek; however, along the eastward projection of the McLeod Creek fault we infer an inactive, buried thrust fault trace based on the uplift of the Plio-Pleistocene alluvial gravels relative to the north. Less than 2 km to the east of the active thrust faults, across the Cache Creek drainage, the evidence for active faulting is expressed as normal faults (Fig. 5).

These active normal faults, collectively referred to as the East Fork faults (Plafker et al., 1994), demonstrate a consistent south side down sense of dip-slip displacement that is continuous from Cache Creek eastward to the Muldrow Glacier (Fig. 6). The scarps of these normal faults follow a fairly linear trace across topography, indicating a near vertical fault dip. However, where these faults cross transverse ridges, the trace is deflected slightly northward, indicating a steep dip to the south. Where the scarp of the southern East Fork fault is continuously preserved across a ridge, a 3-point calculation shows this fault has a steep, southeastward dip of 83°. The normal displacements of the East Fork faults oppose the general south-side-up topographic and geologic expression of the Peters Dome foothills. Even with the reconnaissance-scale of previous mapping (Reed, 1961; summarized and reinterpreted by Wilson et al. (1998) on Fig. 3), the juxtaposition of older units south of the northern East Fork fault against Plio-Pleistocene alluvial deposits on the north demonstrate that the south-side-down motion across the East Fork faults is not the long-term sense of

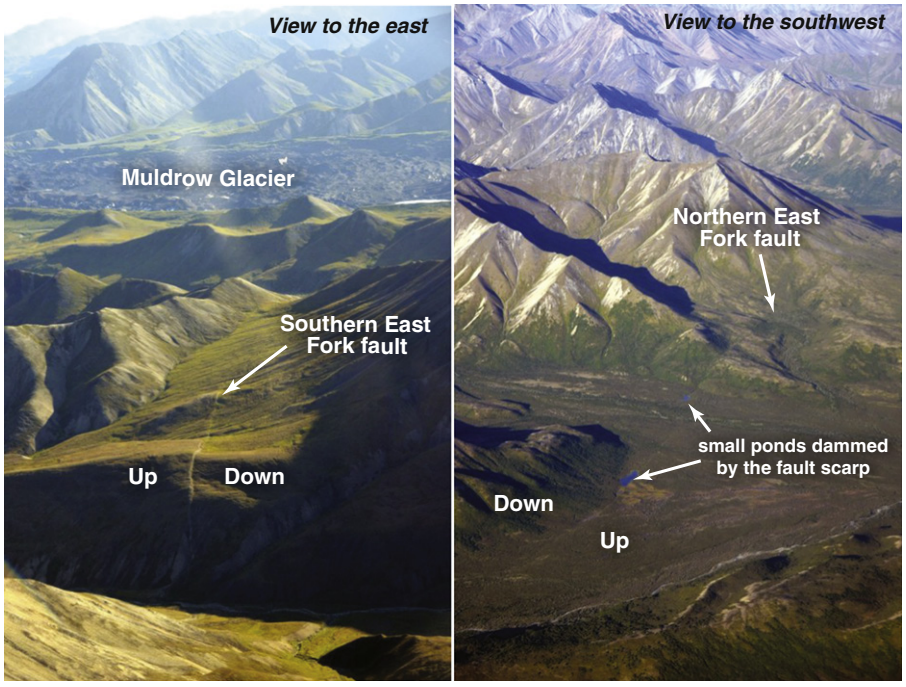

Fig. 6. Oblique photos of the Southern (left) and Northern (right) East Fork fault scarps. Up/down refer to the sense of offset illustrated by the late Pleistocene and Holocene fault scarps. For both faults this displacement produces a 'mountain-side-down' relative motion, and the very steep southward dip shown by the trace Southern East Fork fault across topography indicates a small amount of extension is occurring across this portion of the Peters Dome foothills.

displacement. Although we recognize that the longer-term, bedrock trace of this fault (Fig. 3) extends westward past Cache Creek based on previous bedrock mapping (Reed, 1961), there is no evidence of recent displacement of the same sense as the East Fork faults west of Cache Creek.

Previous mapping indicates that the bedrock geology also transitions abruptly west of Cache Creek with the Cantwell Formation mapped to the north of the geomorphic trend of the northern East Fork fault (Figs. 3 and 5), whereas the Nenana Gravel is mapped north of the northern East Fork fault to the east (Reed, 1961). Although geologic exposure is relatively poor for both of these mapped units north of the northern East Fork fault, field observations during summer 2015 support the previous unit identification. A north-south oriented transverse fault within the Cache Creek drainage could accommodate this transition between the Cantwell Formation and Nenana Gravel as well as accommodate the rapid east-west transition in active faulting styles observed across Cache Creek.

8.2. West of the eastern vertex

The width of the Peters Dome foothills expands and is dominated by thrust fault-related deformation west of the restraining bend eastern vertex (Fig. 5). These thrust faults are generally parallel to the stepover segment of the Denali fault and correspond with major topographic steps within the Peters Dome foothills. The Peters Dome fault is the most outboard of these faults and occurs as a south-dipping thrust fault underlying an uplifted region of Plio-Pleistocene gravels with a plateau-like geomorphic surface on top (Fig. 5). This surface is interpreted as the preserved basin surface prior to initiation of the Peters Dome fault, indicating at least 500 m of vertical slip on this fault. The topographic and structural trends of the Peters Dome fault and the Plio-Pleistocene gravels ends abruptly to the east where the deformation front steps back towards the Denali fault. We interpret this truncation to correspond with a transverse fault connecting the Peters Dome fault with the next active thrust fault to the east, the Northern Slippery Creek fault. This fault does not have a well-defined fault scarp, but is defined based on trends in folding and uplift of Plio-Pleistocene alluvial deposits.

South of the Northern Slippery Creek fault is the westward continuation of the McLeod Creek fault that roughly follows a continuous bedrock fault mapped by Reed (1961) as extending across our entire map area (Fig. 5). Between Peters Glacier and Slippery Creek the McLeod Creek fault is clearly defined by continuous fault scarp segments and the sinuosity of the scarp across intervening ridges indicates a shallow to moderate fault dip (Figs. 5 and 7). In a large, actively raveling stream cut adjacent to McLeod Creek, we measured a dip for the McLeod Creek fault of 45° SE within a ~20 m wide shear zone with a dominant shear fabric sub-parallel to the slip surface. In the footwall below the shear zone there is a zone of brecciated and sheared rock with a sub-vertical fabric, appearing to be kinematically separate from the McLeod Creek fault shear zone. We interpret the sub-vertical shear zone as the inactive trace of the bedrock fault mapped by Reed (1961), suggesting that the McLeod Creek fault is crosscutting this fault rather than reactivating an older steeply-dipping fault.

To the southwest the McLeod Creek fault diverges into two separate faults, the Birch Creek fault to the south and the Chedotlothna fault to the north (Fig. 5). The Chedotlothna fault does not exhibit recent fault scarps within the map area, but the approximate surface trace of the fault is evident from folding of the Plio-Pleistocene gravels. Furthermore, a geomorphic surface on the hanging wall of this fault is similar to the plateau surface on the hanging wall of the Peters Dome fault but with ~0.5 km vertical displacement between the two surfaces. The Birch Creek fault continues along the trend of the previously-mapped continuous bedrock fault of Reed (1961) from the McLeod Creek fault, forming an abrupt boundary between the local bedrock and the Plio-Pleistocene gravels. There is a large geomorphic scarp where this fault appears to cross the southern end of the uplifted geomorphic surface on top of the Plio-Pleistocene alluvial deposits and, due to the interpreted trace of the fault across topography, suggests a moderate southeast dip for this fault. Otherwise, the trace of the Birch Creek fault is predominantly covered by active talus slopes and recent glacial deposits (Fig. 5). We suspect that this fault, as opposed to the McLeod Creek fault, may be the expression of a locally reactivated section of

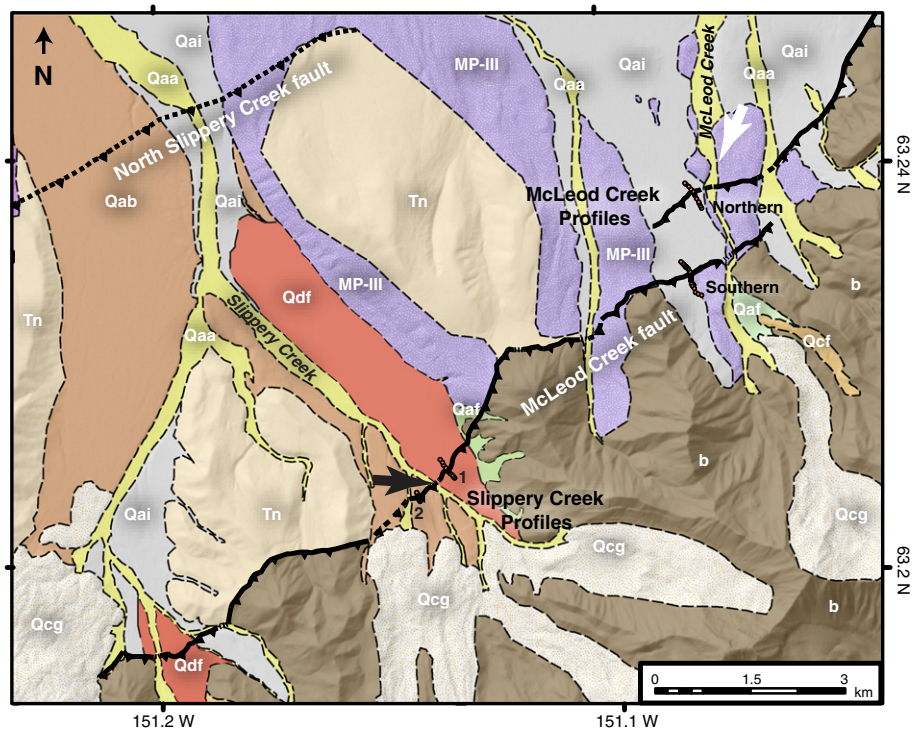

Fig. 7. Quaternary geologic map of a portion of the McLeod Creek fault. Topographic profiles across the McLeod Creek fault scarp near Slippery Creek (labeled 1 and 2) and McLeod Creek (labeled northern and southern) are shown in Fig. 8. Map units are defined in Table 1. Area of map shown on Fig. 5. Black arrow shows approximate orientation and location of the photograph in Fig. 9. White arrow shows view direction and location of the photograph in Fig. 10.

the Reed (1961) bedrock fault due to the steeper dip indicated by the Birch Creek fault trace that mimics the trace of the previous mapping.

8.3. Quaternary fault slip rates north of the vertex of the MMRB

To provide constraints on late Quaternary deformation rates in the Peters Dome foothills, we targeted two locations to establish slip rates along the McLeod Creek fault. These sites were selected due to accessibility and the scarps displace geomorphic surfaces that are clearly correlative across the fault. The expression of the McLeod Creek fault in the east fork of the Slippery Creek drainage consists of a ~1 km continuous scarp across the glacial outwash surfaces forming the valley floor (Fig. 7). The sinuous trace of the fault scarp as it traverses the ridge to the east suggests a relatively low dip angle and we used the 3D expression of the fault scarp across a terrace riser to measure a dip of 25° SE. To document the displacement across this portion of the fault, we collected three topographic profiles using a Trimble GeoXH differential GPS across the scarp and used them to calculate fault dip-slip displacements of 4.4 ± 0.8 m (Slippery 1) and 2.6 ± 3.6 m (Slippery 2) (Fig. 8; methods for calculation and uncertainty estimate provided in Appendix A). Slippery 1 measures the scarp across the surface of unit Qdf, a thin (1–2 m thick in streamcut exposures) debris flow deposit emplaced upon the older fluvial and alluvial gravels of the valley floor. A ~10 cm thick organic-rich fine sand to silt horizon occurs below Qdf and was the ground surface at the time of the debris flow. Qdf and the underlying organic horizon are both deformed the same amount where exposed in a streamcut across the fault scarp, indicating a single earthquake is recorded by this scarp. We isolated 4 distinct organic fractions from the buried organic-rich horizon, resulting in charcoal ages clustered around 3300 cal BP and an age of ~630 cal BP for a collection of fragments of plant macrofossils (Table 3). We interpret that the plant macrofossil age is the best estimate for the age of the soil at the time it was overridden by the debris flow and that the charcoal ages simply record a single prehistoric fire event. The other profile (Slippery 2) was measured along a short, dissected alluvial surface that was unaffected by the debris flow deposits, but exhibits a similarly sized fault scarp. Due to the young age of the debris flow surface, these scarps likely record the displacement from a single earthquake and are not useful for slip rate calculations.

The McLeod Creek fault within the McLeod Creek valley consists of two overlapping strands approximately 0.75 km apart across the same complex alluvial surface (Fig. 7). The smaller, northern scarp ends on the west side of the McLeod Creek valley but is continuous beyond the east side of the valley, where it becomes the primary trace of the McLeod Creek fault. The southern scarp corresponds with offsets of higher, older geomorphic surfaces and is the primary trace of the McLeod Creek fault from McLeod Creek to the west. Both scarps exhibit bending-moment grabens along the crests of the scarps that are predominantly parallel with the scarp. This parallelism and the lack of lateral offset of bar-and-swale fluvial topography across the fault scarp indicate that the recent displacement of this fault is effectively pure dip-slip. We surveyed topographic profiles perpendicular to each fault scarp and, using the measured dip for the McLeod Creek fault nearby and the methods and uncertainty estimation described in Appendix A, determine a fault dip-slip separation of 19.1 ± 2.3 m for the southern scarp and a fault dip-slip displacement of 1.6 ± 3.7 m for the northern scarp (Fig. 8). We interpret that these two scarps connect at depth and their combined offset (20.7 ± 6.0 m) represents the cumulative displacement of this alluvial surface across the McLeod Creek fault since its formation. The alluvial surface offset by these scarps is not directly dated, but the position of the surface upstream from the latest Pleistocene terminal moraine deposits indicates that this surface postdates MP-III (Fig. 5 and Table 2). Due to the dynamic nature of proximal glacial outwash, we expect that this alluvial surface was not abandoned until after the end of the glacial advance at 12.3 ka (Table 2).

We use these fault slip separations derived from topographic profiles across the McLeod Creek fault to provide the first slip rate controls for a component of the MMRB north of the Denali fault. Our data from Slippery Creek do not contribute to the slip rate for this fault because with

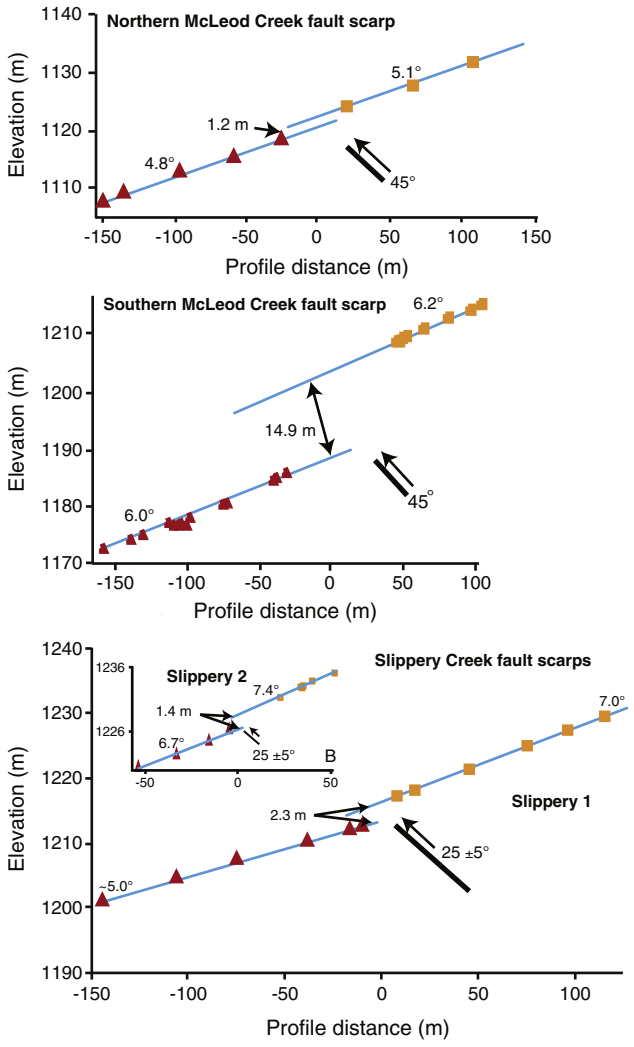

Fig. 8. Surveyed topographic profiles across the McLeod Creek fault at Slippery Creek and McLeod Creek. Point spacing and profile length were dependent upon the extent of the preserved geomorphic surface. The vertical component of fault slip is shown for each scarp. Subsurface fault dips are shown schematically with observed values noted. Profile transects shown on Fig. 7. See Appendix A for the calculations and uncertainty estimate methods.

evidence for a single, young earthquake, there are no closed time intervals between earthquakes from which to calculate a slip rate. Without a direct age on the faulted alluvial surface in McLeod Creek, we are limited to establishing a minimum slip rate based on the 12.3 ka maximum age for the alluvial surface. With the combined offset at McLeod Creek of 20.7 ± 6.0 m, we calculate a minimum slip rate for the McLeod Creek fault of 1.7 ± 0.5 mm/yr. To relate the slip rate of the McLeod Creek fault to the to the strike-slip deformation on the Denali fault, we convert these slip rates into horizontal shortening rates. These rates define limits on the amount of contraction across the Peter Dome foothills and parallel to the Denali fault west of the eastern vertex. The McLeod Creek fault minimum horizontal shortening rate is 1.2 ± 0.4 mm/yr, oriented perpendicular to the fault trace.

9. Seismicity linked to the MMRB

Seismicity associated with the Kantishna cluster covers an irregularly shaped region extending from the Denali fault north to the Kantishna Hills (Fig. 11). The portion of this seismicity that occurs within the Peters Dome foothills is restricted to the west of the eastern vertex of the MMRB. The persistent low-magnitude seismicity has exhibited earthquake rates much higher than regional background seismicity rates for the duration of regional seismic monitoring, with over 18,000 recorded earthquakes (of magnitudes ranging from <1 to 5.2) in the last 48 years. Detailed analysis of the Kantishna cluster by Burris (2007) identified 3 primary subzones of seismicity, north, middle, and south, which are delineated based upon diffuse, elliptical clusters of seismicity with different orientations of these clusters relative to the Denali fault (Fig. 11; Ruppert et al., 2008; Burris, 2007). Furthermore, stress tensor inversions on focal mechanisms for each subzone illustrate a general pattern of NW–SE oriented maximum compressive stress, although the orientation and inferred style of faulting vary between each zone (Burris, 2007).

We obtained the catalog of earthquakes recorded in the Kantishna cluster from 1986 to 2013 from the Alaska Earthquake Information Center to analyze the regional seismicity in the context of our new Quaternary geologic mapping (Fig. 5). To test for associations between the seismicity and our newly recognized faults, we examine cross-sections of the seismicity across the middle and south subzones. If the local background seismicity primarily occurs on the mapped active faults, we predict that these cross-sections will display trends of seismicity that project to the surface trace of the fault.

9.1. MMRB seismicity trends

The distribution of epicenters for the middle subzone forms an ellipsoidal region that is elongate along an E-W axis, with focal mechanisms showing predominantly reverse slip. Strike-slip focal mechanisms are also common in this subzone and these exhibit an orientation of the maximum compressive stress that is consistent with the reverse focal mechanisms of the same subzone. (Fig. 11). The seismicity of the

Table 3
Radiocarbon analyses from deformed buried soil at slippery creek.

Sample name[a]	CAMS lab number[b]	^{14}C age (BP)[c]	Calibrated age (cal BP)[d]	Sample material[f]	Sampled unit	Interpretation
MMRB01-A	166184	3130 ± 140	3685–2960	Seeds? (a)	Buried soil	Inherited charred material
MMRB01-B	166185	>Modern	NA	Very fine roots (b)	Buried soil	Modern roots
MMRB01-C	166186	630 ± 70	684–525	Wood/twigs/old roots	Buried soil	Recent plant growth at time of debris flow
MMRB01-D[e]	166187	3065 ± 25	3359–3210	Charcoal (c)	Buried soil	Inherited charcoal
MMRB01-F	166188	3140 ± 60	3480–3182	Charcoal (c)	Buried soil	Inherited charcoal

Note: Samples were picked from a block soil sample at the University of Kentucky and the sent to Lawrence Livermore National Laboratories Center for Accelerator Mass Spectrometry (LLNL CAMS) for AAA pretreatment.

[a] Site name codes: MMRB = Mt. McKinley Restraining Bend; 01 = block sample #1; A–F = organic fractions separated from the block sample.

[b] AMS analysis performed at LLNL CAMS.

[c] The quoted age is in radiocarbon years using the Libby half-life of 5568 years and following the conventions of Stuiver and Polach (1977). Sample preparation backgrounds have been subtracted, based on measurements of radiocarbon-dead standards pretreated in parallel with samples.

[d] Ages calibrated with Oxcal v4.2 (Bronk Ramsey, 2009a) using the IntCal 13 calibration curve (Reimer et al., 2013), with ages quoted at 2σ errors.

[e] Sample was large enough to take a sample specific aliquot for ^{13}C analysis.

[f] (a) black, charcoal-like spheres — possibly seeds. (b) collection of fine roots penetrating the buried soil horizon. (c) inherited charcoal preserved within the soil.

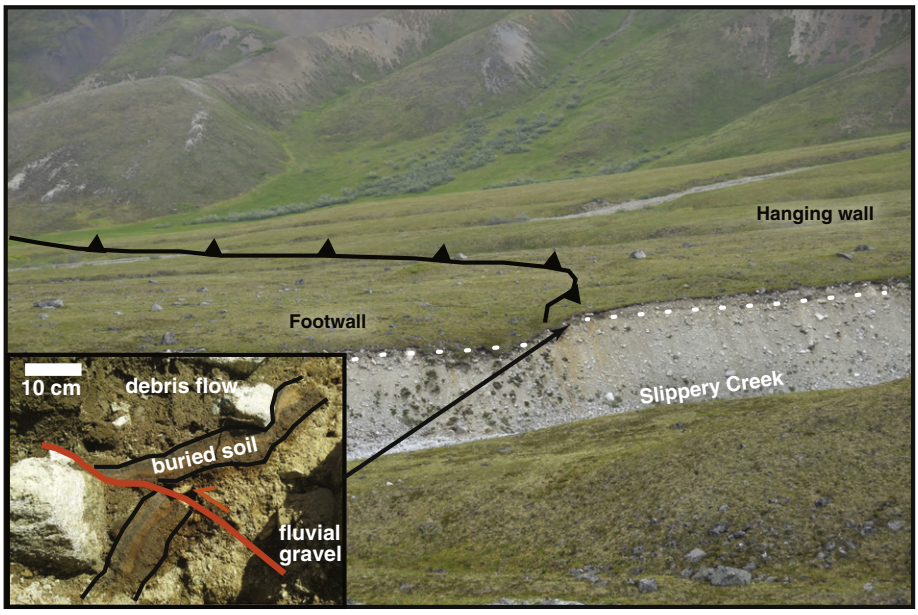

Fig. 9. Slippery Creek fault scarp exposure. Looking east along the trace of the McLeod Creek fault, the fault offsets the surface of a debris flow deposit. A stream cut across the fault scarp exposes a thin, buried soil that separates the debris flow deposit from the underlying fluvial deposits (inset photo). This buried soil is offset (white dotted line in main photo) and deformed across the scarp with a geometry that mimics the surface scarp. Location of photo shown on Fig. 7.

south subzone follows the NNE–SSW trend of the Peters Dome foothills and the epicenters appear exclusively between the surface traces of the Peters Dome/Chedotlothna faults and the Denali fault (Fig. 4). Many focal mechanisms of this zone indicate reverse slip perpendicular to the Denali fault with additional lateral-slip focal mechanisms, particularly closer to the Denali fault. Relative to the abundant seismicity west of the eastern vertex of the MMRB, background seismicity is nearly absent from the Peters Dome foothills to the east of this vertex (Figs. 4 and 11).

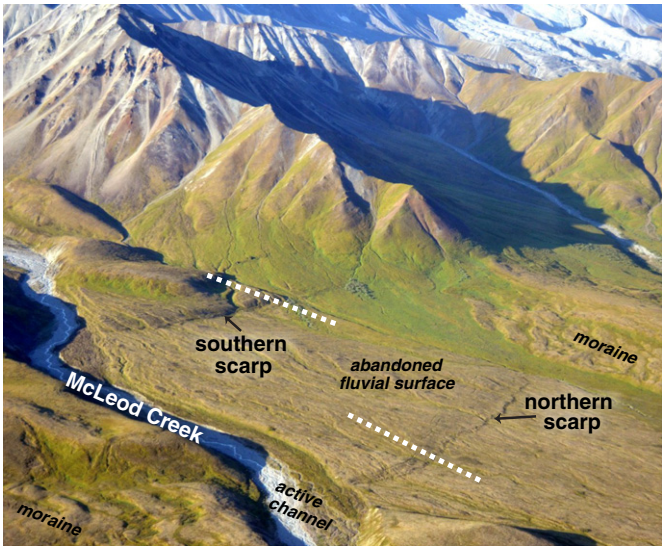

Fig. 10. Fault scarps of the McLeod Creek fault across the McLeod Creek valley. Southwest looking photo illustrates the overlap zone between the two traces of the McLeod Creek fault and the relationship with surficial geologic units. Preserved channels and bar/swale topography of the abandoned fluvial surface do not illustrate any lateral offset across these fault scarps. Dashed white lines show the topographic profiles transects across these fault scarps. Location of photo shown on Fig. 7.

9.2. Subsurface fault geometry based on regional seismicity

The diffuse map-view pattern of earthquake epicenters in the Kantishna cluster could simply be the expression of one or more dipping thrust faults with the seismicity distributed along the fault planes. To test this scenario, we extracted cross-sections across the subzones of seismicity. With the elliptical shape of these zones, one cross section was taken along the long axis and two additional cross sections were extracted either perpendicular to the Denali fault or through the densest portions of the cluster. The first set of cross sections include all ~18,000 hypocenters that were recorded from 1968 to 2013 (Figs. 11 and 12). In general, all cross-sections across the south and middle zones exhibit diffuse seismicity at all depths. A few weak patterns emerge visually in the data but robust trends that could represent discrete fault planes are not apparent. However, if the diffuse seismicity is a product of poor hypocentral locations, filtering this dataset may reveal hidden fault planes. As a simple refinement of this dataset, we used characteristics of the earthquake catalog and seismic network to select the hypocenters that should have a greater accuracy. In consideration of our attempt to differentiate subsurface faults over distances of 5–10 km, we selected only hypocenters with a stated average horizontal and vertical error less than 1 km. Temporally, we exclude data older than 2005 because this time represents the conclusion of several seismic network upgrades, thus earthquakes occurring after 2005 should have the best network coverage of the catalog (e.g., Ruppert et al., 2008). Finally, we exclude hypocenters with a magnitude less than 2 because of the correspondence of smaller location errors with increased magnitude. The resulting cross sections of the filtered data still show diffuse zones of seismicity, although additional depth clustering and weak dipping trends are visually apparent (Fig. 13). For example, the hypocenters of the C–C′ and E–E′ cross sections have overall north and northwest dipping (respectively) subsurface trends, but the scatter that remains in the seismicity trends make interpreting a fault plane dubious. Additionally, these trends do not correlate with the surface constraints for any mapped active faults (Fig. 13). Given our inability to make connections between subsurface seismicity trends and patterns of active faulting observed on the surface, we suspect that the earthquakes of the Kantishna cluster are either, 1) occurring primarily on

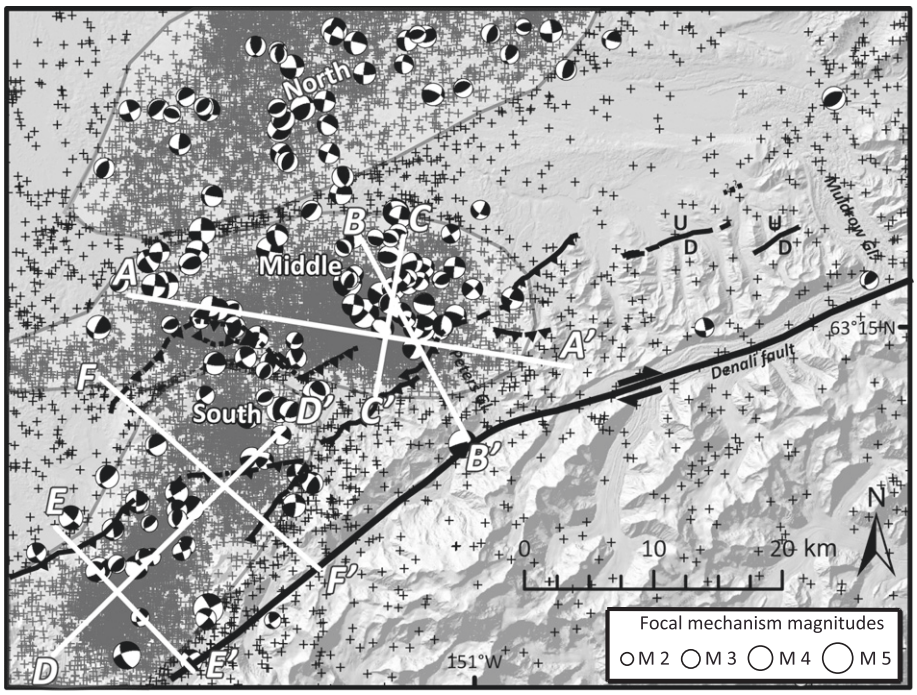

Fig. 11. Shallow crustal seismicity patterns near the Mount McKinley restraining bend. Previous studies divide the seismicity of the Kantishna cluster into north, middle, and south zones (Burris, 2007; Ruppert et al., 2008). Background seismicity is notably sparse to the east of the eastern vertex, along the trace of the Denali fault, and south of the Denali fault. Seismicity shown for 1968–2013 with depths of <25 km, although most hypocenters occur at <15 km depth. Focal mechanisms for this time period exhibit predominantly reverse and strike-slip displacements. White lines show the section lines for the seismicity cross-sections in Figs. 12 and 13.

the major active fault planes but hypocenter locations are too poorly located to clearly define these fault planes, or 2) occurring primarily off the major active fault planes such that the distributed seismicity truly is diffuse.

10. Discussion

10.1. How does the MMRB persist?

Late Quaternary fault activity along the north side of the Denali fault through the restraining bend exhibits a persistent pattern of shortening adjacent to the stepover fault in contrast to the lack of deformation or fault perpendicular extension that occurs east and west of the restraining bend. In particular, the change in structural style from steeply-dipping normal faults to low/moderately dipping thrust faults requires a major shift in the local stress field adjacent to the eastern vertex of the MMRB (Fig. 5). The Denali fault-parallel, south-dipping normal faults suggests a vertical maximum compressive stress and a near horizontal minimum compressive stress that is oriented perpendicular to the Denali fault. Denali fault-parallel thrust/reverse faults occur along the entire stepover fault segment, suggesting that the maximum compressive stress is near horizontal and oriented perpendicular to the Denali fault and the minimum compressive stress is vertical. These interpretations of stress orientations suggests that the local stress field undergoes a ~90° rotation about a horizontal axis and ~20° rotation about a vertical axis and this occurs over a short distance (<5 km) in the crust adjacent to the eastern vertex of the MMRB. This transition, near Cache Creek (Fig. 5), occurs 10–15 km east of the eastern vertex due to the curvature of the bend in the Denali fault and the elastic properties of the crust. The eastern limit of the clustered background seismicity (Figs. 4 and 11) roughly corresponds with this change in stress field, suggesting a possible relationship between the crustal processes occurring west of the stepover fault segment and the source of the elevated seismicity.

Longer-term (pre-late Quaternary) geologic relationships suggest that this along-strike change in the local stress field is a relatively recent phenomenon. Occurrences of Plio-Pleistocene alluvial gravels, such as those in our map area (Figs. 3 and 5), throughout the Alaska Range typically appear on the hanging wall of thrust faults and within thrust fault-related folds (e.g., Bemis et al., 2012; Bemis and Wallace, 2007; Wahrhaftig, 1987). Because the thrust faults uplift the alluvial gravels above base level of the adjacent basin, the presence of this unit is a key marker indicating Quaternary contraction along the northern flank of the Alaska Range. We map the Plio-Pleistocene alluvial gravels across our map area of the Peters Dome foothills (Fig. 5); however, these deposits appear in the hanging wall of active thrust faults in the west and in the footwall of a normal fault (Northern East Fork fault) in the east. Although there is no clear surface trace of a thrust fault that defines the northern margin of these eastern exposures of alluvial gravels (Fig. 5), we infer the presence of an inactive, buried thrust fault trace along the eastward projection of the McLeod Creek fault which formerly accommodated uplift of the Plio-Pleistocene gravels and adjacent foothills. Furthermore, the occurrence of Eocene plutonic rocks in the hanging wall of the Northern East Fork fault over the Plio-Pleistocene alluvial gravels indicate a period of contraction across this fault prior to the late Quaternary phase of extension (Figs. 5 and 14). Together these two thrust faults accommodated early to mid-Quaternary shortening and are now either inactive or reactivated as extensional in the modern local stress field.

Based on these inferred stress variations across the north side of the restraining bend, we interpret that the contractional deformation of the MMRB is primarily controlled by the response of lateral crustal motion interacting with the oblique (stepover) portion of the Denali fault. Furthermore, the temporal change from contractional to extensional fault behavior along the East Fork faults (Fig. 14) suggests that the contractional deformation of the MMRB has migrated southwest along the Denali fault to its current position. Preliminary low-T thermochronologic data also support a southwest-migrating focus of contractional deformation with cooling ages becoming progressively younger on both sides of the Denali fault towards the MMRB eastern vertex (Fig. 3; Bemis et al., 2015a,b; Terhune et al., 2014). Existing models of migrating restraining bends (e.g., Wakabayashi, 2007) typically illustrate the

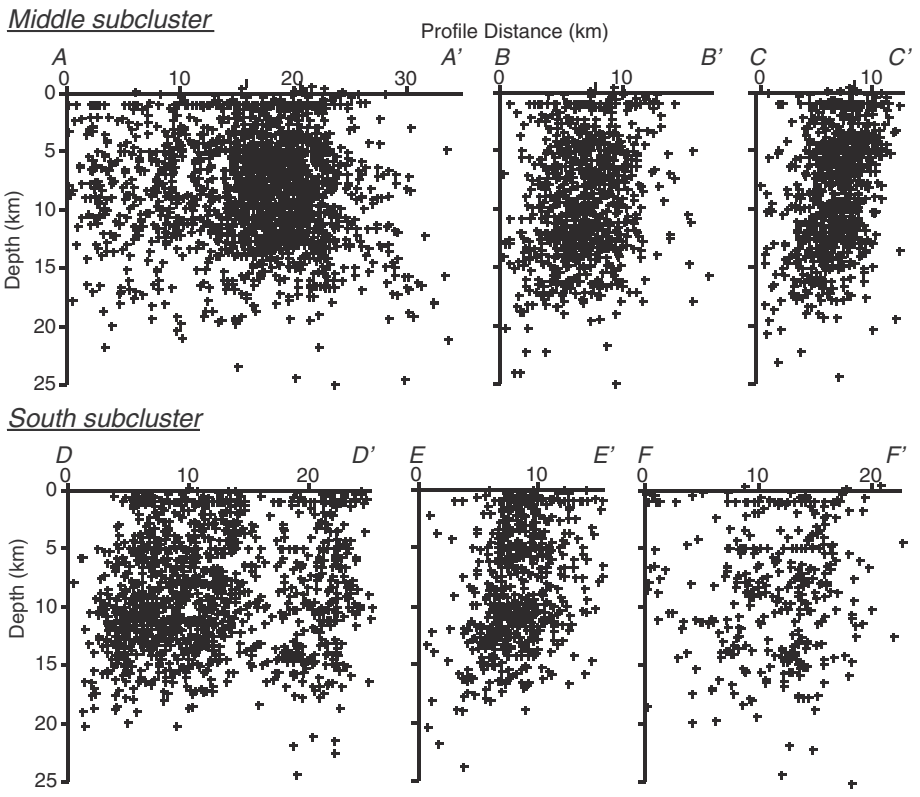

Fig. 12. Cross-sections of shallow seismicity for the middle and south zones of the Kantishna cluster. Hypocenters sampled from 2 km wide swaths along the lines of sections shown on Fig. 11. Weak patterns are apparent, but the character is predominantly diffuse seismicity across the entire depth range.

progressive creation of new stepover fault segments to accommodate the along fault migration of a restraining bend (Fig. 1). These new stepover segments act to slice off portions of crust from one side of the fault and incorporate it into the other side of the fault, producing a migration of the restraining bend in the direction that new stepover segments are produced (Fig. 1). Existing geologic mapping (Reed, 1961; Reed and Nelson, 1980; Wilson et al., 1998; unpublished mapping generalized in Haeussler, 2008) does not support the existence of abandoned stepover faults. Although the "Foraker thrust fault" of Haeussler (2008; Fig. 4) is in a logical position to potentially be a former stepover segment, Haeussler (pers. comm., 2015) indicates all fabrics near the fault are consistent with thrust-related deformation. Additionally, the southern portion of this fault is pinned by two plutons correlated with the early Cenozoic McKinley Sequence (Lanphere and Reed, 1985) which places limits on potential strike-slip motion (Fig. 3; Reed and Nelson, 1980; Wilson et al., 1998). Finally, the potential for unidentified major faults through the MMRB that could be abandoned stepover faults is very limited due to the relatively narrow zones that exist between the large, unfaulted plutons. Hence, we propose a new process to accommodate along-fault migration of gentle restraining bends based on the deformation pattern demonstrated by the MMRB.

Our current evidence for the occurrence of, and potential mechanism for, migration of the MMRB eastern vertex (relative to previously deformed deposits) is based on the 'tectonic wake' of previously shortened deposits that are now undergoing extension and geometric constraints presented by the major active structures of the MMRB. These primary geometric constraints are the orientation and transport direction of active thrust faults adjacent to the stepover segment, the Denali fault occurs as a backstop to these active thrust faults, and the orientation of the Denali fault east of the stepover segment (Fig. 14). With this configuration, as displacement accumulates on the northwest-vergent thrust faults, the stepover segment of the Denali fault is translating to the northwest in the hanging wall of the thrust faults. Simultaneously, new material enters the MMRB from the east and is transported into the bend, where it is translated both up the northwest-vergent thrust fault and laterally along the Denali fault (Fig. 15). Considering the linear trace of the Denali fault east of the bend, the movement of the projected intersection between the translating stepover fault segment and the trace of the Denali fault from east of the bend defines the migration of the MMRB eastern vertex. The result is a 'rolling hinge' style migration of the bend vertex towards the southwest (Fig. 15).

Using our model of restraining bend evolution and basic constraints on fault geometry, we use our slip rate estimates for the northwest-vergent thrust faults and existing Denali fault slip rate constraints from east of the MMRB to calculate the migration rate for the eastern vertex of the bend (Fig. 15). In a reference frame that holds the north side of the Denali fault fixed, the Denali fault slip rate from east of the MMRB (DF_t = 7–9 mm/yr; Haeussler et al., 2012; Mériaux et al., 2009) represents the rate at which crust enters the bend. Within the bend, this motion is partitioned into the Denali fault stepover-parallel rate (a), the stepover-perpendicular rate (Tf), and the vertex migration rate (b) (Fig. 15). Using intermediate values for our constrained slip rates Df_t and Tf, our (a) and (b) unknowns are both ~4 mm/yr. The full range of vertex migration rates and Denali fault stepover segment-parallel slip rates based upon the estimates of Df_t and Tf is 2–6 mm/yr and 3–5 mm/yr, respectively (Fig. 15). Within our simple geometric framework, the range of Denali fault stepover segment-parallel slip rate varies only with the range of Tf values whereas the migration rate varies with both Tf and Df_t rates. As a result, inclusion of an inferred (albeit unconstrained) component of shortening occurring on the S and SW-striking thrust faults south of the Denali fault shown on Fig. 3 (Hauessler, 2008; Reed and Nelson, 1980) predicts that the vertex migration rate should be at the low end or below our calculated range.

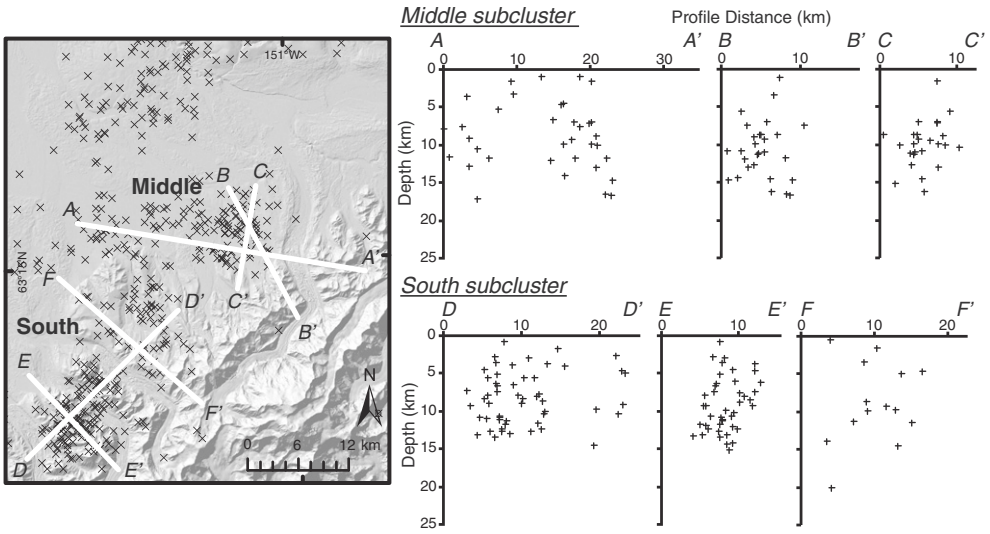

Fig. 13. Cross-sections of the filtered shallow seismicity for the middle and south zones of the Kantishna cluster. Only earthquakes >M2 and during 2005–2013 are shown to illustrate hypocenters with the highest location accuracy. Earthquakes are sampled from a 2 km wide swath centered on each transect. Some weak trends in hypocenter clusters appear to illustrate dipping and vertical zones of seismicity, but most of these weak patterns have widths of >5 km and do not appear to provide interpretable constraints on subsurface geometry of our mapped active faults. White lines show the locations of the cross sections.

Shortening on these faults is expected as a mechanism for structural uplift of the high topography within the MMRB, but rates are unconstrained due to a lack of Quaternary markers associated with these faults. Our rates will be refined with future Quaternary geochronology currently in progress on deposits throughout the MMRB. Furthermore, these rates represent late Quaternary controls on fault slip rates and the migration rate of the MMRB, and we expect future results from ongoing thermochronologic and structural studies to establish slip and migration rate constraints over longer intervals to illustrate whether these rates are changing through time.

Our model of a migrating MMRB appears to be in conflict with the typical association of sustained focused uplift with fixed restraining bends. The presence of the high topography associated with Denali and Foraker suggests that the focused rock uplift is maintained by mechanisms other than the stationary position of a restraining bend. Four likely interrelated mechanisms acting to drive persistent rock uplift in the MMRB are: 1) asymmetric development of topography associated with gentle restraining bends restricts the contractional component of deformation to a narrower zone, 2) a ~75 km long restraining stepover segment means that once a piece of crust moves into the bend, it will remain in the region of contraction for millions of years, 3) if the stepover fault segment persists, the focused uplift is not abandoned by the creation of new stepover segments that occurs in traditional migrating restraining bends, and 4) potential fault geometries required to maintain the same fault trace through the restraining bend while simultaneously translating it require the involvement of a dipping fault that would additionally drive rock uplift adjacent to the stepover segment.

10.2. Implications for earthquake behavior through a migrating gentle restraining bend

The role of geometric complexities in strike-slip faults, such as fault stepovers and restraining bends, in impeding earthquake ruptures has long been debated (e.g., Schwartz and Coppersmith, 1984, 1986; Schwartz and Sibson, 1989; Wesnousky, 2006; Yıkılmaz et al., 2014). The discrete 18° bend of the eastern vertex of the MMRB lies at the modeled and observed threshold where restraining bends with a greater bend angle will limit rupture propagation (Elliott et al., 2015; Lozos et al., 2011). Unfortunately, we cannot provide new paleoseismic data from the MMRB to further test these predictions of rupture propagation due to >100 km of continuous coverage of the Denali fault trace by glaciers and active talus. However, the slip rate decrease to the west through the restraining bend suggests that either the Denali fault to

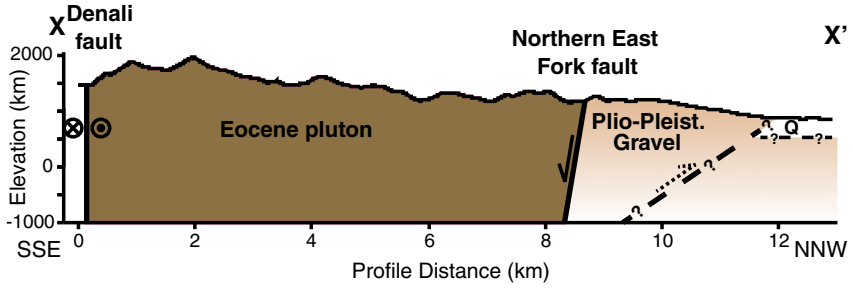

Fig. 14. Schematic cross-section across the Northern East Fork fault illustrating the geologic relationships in the Peters Dome foothills east of the eastern vertex. Subsurface fault dips are not well constrained but shown to represent basic field relationships. The Northern East Fork fault is a normal fault, but the older over younger relationship across the fault indicates that this fault was previously a contractional structure. We do not see a direct surface trace of the inferred thrust fault, but the uplift of the Plio-Pleistocene gravel above local base level and correspondence with the topographic range front suggests the presence of a formerly active fault in this configuration.

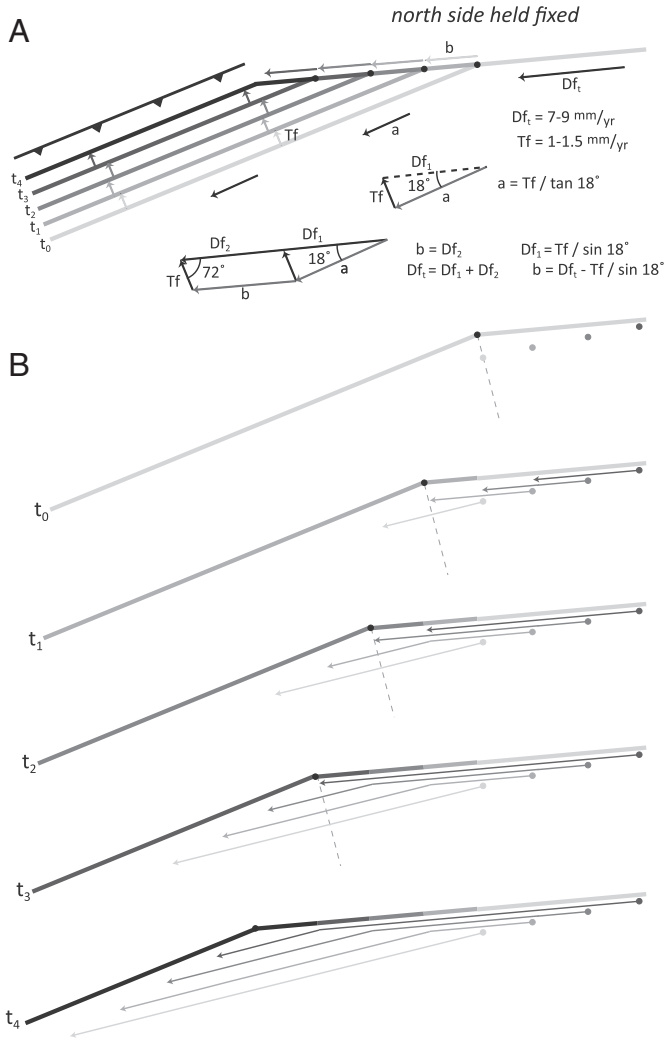

Fig. 15. Schematic model of restraining bend migration for the MMRB. (A) Snapshots of our proposed migration progression of the Denali fault surface trace due to displacement on the adjacent thrust faults. The lightest gray (t_0) represents an initial condition and progressively darker lines depict the position of the fault trace at subsequent points in time. Total slip entering the restraining bend (DFt) is partitioned into a Denali fault-parallel component (a), Denali fault-perpendicular component (Tf), and the migration of the restraining bend apex (b). Diagram shown with calculations depicted at 2× scale for legibility. Grayscale arrows depict the motion of geometric entities (restraining bend vertex and the stepover fault segment) at each time step. Note that each time step represents the translation of the Denali fault surface trace, not the formation of new faults. (B) Development of particle paths through the restraining bend for particles entering the bend at each migration step shown in (A). Paths drawn to represent the same time period but with different starting positions so that each particle passes into the restraining bend at the time corresponding with their color. These paths do not include shortening occurring within the MMRB. Shortening across the previously mapped S and SW-striking thrust faults south of the Denali fault (Fig. 3) would reduce the west component of the particle paths, producing greater curvature of the particle paths to the southwest.

the east of the MMRB experiences more frequent surface-rupturing earthquakes, there is a persistent pattern of lower displacements during surface-rupturing earthquakes on the Denali fault west of the MMRB, or some combination of the two. Furthermore, because the southwestward propagation of the eastern vertex of the MMRB is accommodated by displacement across faults adjacent to the primary strike-slip fault, the stepover segment of the MMRB has a lower slip rate than adjacent portions of the Denali fault outside the restraining bend. From this we can predict that some large ruptures of the Denali fault do end within the MMRB, likely acting to promote failure on the subsidiary active faults discussed in this study that accommodate restraining bend migration or the thrust faults underlying Denali (Haeussler, 2008).

11. Conclusions

Our Quaternary geologic mapping on the north side of the Denali fault across the eastern vertex of the MMRB illustrates a fundamental change in near-field crustal deformation associated with the evolution of this fault bend. Quaternary-active faults east of the vertex are predominantly very steeply south-dipping normal faults, whereas those west of the vertex are predominantly gently to moderately dipping thrust faults. Constraints on the maximum cumulative slip rate from offset latest Pleistocene/early Holocene deposits across the thrust faults of ~2 mm/yr indicates a horizontal shortening rate across these faults of 1–1.5 mm/yr. In contrast, the steep >80° dip of the normal faults indicates that the horizontal extension is a small fraction of the cumulative slip. This situation results a relatively fixed geometry of the Denali fault trace east of the bend vertex and a northwestward translating stepover fault segment west of the vertex. This northwestward translation produces a migration of the eastern vertex of the MMRB to the southwest along the Denali fault at a rate of ~2–6 mm/yr.

The distribution and style of the anomalous shallow crustal seismicity of the Kantishna cluster appears to be at least partially controlled by the migration of the eastern vertex of the MMRB. This seismicity does not clearly delineate subsurface fault planes despite the occurrence of discrete, active fault surface traces, suggesting that the background seismicity potentially reflects diffuse deformation occurring between major surface rupturing earthquakes or better seismic network coverage is required to improve hypocentral locations. In contrast, east of the vertex there are fault scarps indicative of surface-rupturing earthquakes, but background seismicity is nearly absent. Therefore, the current localization of this background seismicity west of the vertex further illustrates the change in the stress field that occurs over a relatively short distance reflecting the transition in off-primary-fault deformation across the vertex.

The rapid exhumation and extreme topography of Denali occurs within a gentle restraining bend that is migrating along the Denali fault. Migration of the eastern vertex of the MMRB is accommodated by the northwestward translation of the stepover fault segment of the Denali fault in the hanging-wall of the adjacent active thrust faults. This translation of the stepover fault segment geometrically requires that the eastern vertex of the restraining bend migrate to the southwest. The uncommon association of high topography with a migrating restraining bend likely results from the interplay of the length of the stepover fault segment, the persistence of the stepover fault through time, and uplift that results from the translation of the stepover fault segment. As a result, the prolonged focused uplift within the MMRB that produces the highest topography in North America is due primarily to the amount of time that the crust stays within the zone of contraction adjacent to the stepover fault segment.

Acknowledgements

This research was supported by National Science Foundation award EAR 1250461. This manuscript benefitted substantially from a review by J. Wakabayashi and two anonymous reviewers provided valuable additional guidance. L. Tyrrell and D. Capps of Denali National Park & Preserve provided critical logistical and scientific support. PRISM Helicopters and A. Shapiro of Alaska Land Exploration provided skilled helicopter transport in and out of the field area. P.B. O'Sullivan and J. Metcalf assisted with the preliminary AFT and ZHe data, respectively. Additional thanks to J.K. Carlson, L. DeVore (Walker), and P. Terhune for their assistance in the field and lab.

Appendix A

Slip rate errors were estimated using a bootstrap resampling approach with a bootstrap sample of the data for each elevation profile of elevation (y) data was collected in R statistical software, where a resampling of the elevations that define the hanging wall and footwall is completed to delineate 50 different elevation samples for each profile. Each sample of the 50 was then used to calculate the Simple Linear Regression slope and y-intercept coefficients. These coefficients were then used to compute the fault slip. Then, assuming that the bootstrap sample estimate approximates a normal distribution, we calculated the standard deviation and mean of the bootstrap estimates to obtain the estimate and standard error. Because little is known about the statistical distribution of the estimates and the sample set was small, we could not use traditional methods to approximate the standard error.

Given the regression uncertainty, meter-scale surface irregularities, and short profile distances, slopes within two degrees are considered parallel. The surveyed points of the topographic profiles define the hanging wall, the scarp face, and footwall of each scarp. We calculated a linear regression for each hanging wall and footwall set of survey points to establish trend lines through the surveyed points to define the equations representing the hanging wall ($y_h = m_h x + b_h$) and the footwall ($y_f = m_f x + b_f$). These equations give the necessary variables used in the Thompson et al. (2002) vertical and slip offset equations. To calculate the fault slip for a particular scarp, first we calculated the vertical offset of the topographic surface by subtracting the y-intercepts of each fault wall block surface. For parallel surfaces, the vertical offset is $v = b_h - b_f$

Next, using the vertical offset, we determine the dip slip offset on the fault plane from,

$$s = v\cos\alpha / \sin(\alpha + \delta)$$

where v is vertical separation, α is surface dip, δ is fault dip, and $\tan\alpha = m$. If the surface dip (α) of each fault wall block is not the same, then the two numbers were averaged for the dip slip calculation. We calculated fault slip rates by taking the fault dip slip (s) dividing by the age (a) of the fault surface obtained by glacial correlations

$$\text{Slip rate} = s/a$$

Appendix B. Supplementary data

Supplementary data associated with this article can be found in the online version, at http://dx.doi.org/10.1016/j.tecto.2016.05.009. These data include Google map of the most important areas described in this article.

References

Bemis, S.P., Wallace, W.K., 2007. Neotectonic framework of the north-central Alaska Range foothills. In: Ridgway, K.D., Trop, J.M., Glen, J.M.G., O'Neill, J.M. (Eds.), Tectonic Growth of a Collisional Continental Margin: Crustal Evolution of Southern Alaska, Geological Society of America Special Paper, pp. 549–572.

Bemis, S.P., Carver, G.A., Koehler, R.D., 2012. The Quaternary thrust system of the northern Alaska Range. Geosphere 8, 196–205. http://dx.doi.org/10.1130/GES00695.1.

Bemis, S.P., Benowitz, J., Fendick, A., Terhune, P., Carlson, J.K., Burkett, C., 2015a. Advection and migration in the Mount McKinley restraining bend of the Denali fault, Denali National Park & Preserve, Alaska. Geological Society of America Abstracts with Programs, p. 443.

Bemis, S.P., Weldon, R.J., Carver, G.A., 2015b. Slip partitioning along a continuously curved fault: Quaternary geologic controls on Denali fault system slip partitioning, growth of the Alaska Range, and the tectonics of south-central Alaska. Lithosphere L352, 1. http://dx.doi.org/10.1130/L352.1.

Benowitz, J.A., Layer, P.W., Armstrong, P., Perry, S.E., Haeussler, P.J., Fitzgerald, P.G., VanLaningham, S., 2011. Spatial variations in focused exhumation along a continental-scale strike-slip fault: the Denali fault of the eastern Alaska Range. Geosphere 7, 455–467. http://dx.doi.org/10.1130/GES00589.1.

Benowitz, J.A., Bemis, S.P., O'Sullivan, P.B., Layer, P.W., Fitzgerald, P.G., Perry, S.E., 2012a. The Mount McKinley Restraining Bend: Denali Fault, Alaska, in: Geological Society of America Abstracts With Programs (Charlotte, NC) p. 597.

Benowitz, J.A., Haeussler, P.J., Layer, P.W., O'Sullivan, P.B., Wallace, W.K., Gillis, R.J., 2012b. Cenozoic tectono-thermal history of the Tordrillo Mountains, Alaska: Paleocene–Eocene ridge subduction, decreasing relief, and late Neogene faulting. Geochem. Geophys. Geosyst. 13 (22 PP. doi:201210.1029/2011GC003951).

Benowitz, J.A., Layer, P.W., Vanlaningham, S., 2014. Persistent long-term (c. 24 Ma) exhumation in the Eastern Alaska Range constrained by stacked thermochronology. Geol. Soc. Lond., Spec. Publ. 378, 225–243. http://dx.doi.org/10.1144/SP378.12.

Brennan, P.R.K., Gilbert, H., Ridgway, K.D., 2011. Crustal structure across the central Alaska Range: anatomy of a Mesozoic collisional zone. Geochem. Geophys. Geosyst. 12. http://dx.doi.org/10.1029/2011GC003519 (23 PP.).

Briner, J.P., Kaufman, D.S., 2008. Late Pleistocene mountain glaciation in Alaska: key chronologies. J. Quat. Sci. 23, 659–670. http://dx.doi.org/10.1002/jqs.1196.

Burris, L., Ruppert, N.A., Hansen, R.A., 2007. The Structure of the Kantishna Seismic Cluster, Central Alaska, Derived From Stress Tensor Inversions and Seismicity Trends. AGU Fall Meeting Abstracts 43 p. 1043.

Carver, G.A., Bemis, S.P., Solie, D.N., Obermiller, K.E., 2008. Active and Potentially Active Faults in or Near the Alaska Highway Corridor, Delta Junction to Dot Lake, Alaska (Preliminary Interpretive Report No. 2008-3D). Alaska Division of Geological & Geophysical Surveys Preliminary Interpretive Report (32 pp.).

Carver, G.A., Bemis, S.P., Solie, D.N., Castonguay, S., Obermiller, K.E., 2010. Active and Potentially Active Faults in or Near the Alaska Highway Corridor, Dot Lake to Tetlin Junction, Alaska (Preliminary Interpretive Report No. 2010-1). Alaska Division of Geological & Geophysical Surveys.

Coney, P.J., Jones, D.L., 1985. Accretion tectonics and crustal structure in Alaska. Tectonophysics 119, 265–283.

Cooke, M.L., Schottenfeld, M.T., Buchanan, S.W., 2013. Evolution of fault efficiency at restraining bends within wet kaolin analog experiments. J. Struct. Geol. 51, 180–192. http://dx.doi.org/10.1016/j.jsg.2013.01.010.

Crowell, J.C., 1974. Origin of Late Cenozoic basins in Southern California. In: Dickinson, W.R. (Ed.), Tectonics and Sedimentation, SEPM Special Publications, pp. 190–204.

Csejtey, B., Mullen, M.W., Cox, D.P., Stricker, G.D., 1992. Geology and Geochronology of the Healy Quadrangle, South-central Alaska (Miscellaneous Investigations No. 1191). U.S. Geological Survey.

Cunningham, W.D., Mann, P., 2007. Tectonics of strike-slip restraining and releasing bends. Geol. Soc. Lond., Spec. Publ. 290, 1–12. http://dx.doi.org/10.1144/SP290.1.

Dortch, J.M., Owen, L.A., Caffee, M.W., Brease, P., 2010a. Late Quaternary glaciation and equilibrium line altitude variations of the McKinley River region, central Alaska Range. Boreas 39, 233–246. http://dx.doi.org/10.1111/j.1502-3885.2009.00121.x.

Dortch, J.M., Owen, L.A., Caffee, M.W., Li, D., Lowell, T.V., 2010b. Beryllium-10 surface exposure dating of glacial successions in the Central Alaska Range. J. Quat. Sci. 25, 1259–1269. http://dx.doi.org/10.1002/jqs.1406.

Eberhart-Phillips, D., Christensen, D.H., Brocher, T.M., Hansen, R., Ruppert, N.A., Haeussler, P.J., Abers, G.A., 2006. Imaging the transition from Aleutian subduction to Yakutat collision in central Alaska, with local earthquakes and active source data. J. Geophys. Res. 111, B11303. http://dx.doi.org/10.1029/2005JB004240.

Elliott, A.J., Oskin, M.E., Liu, J., Shao, Y., 2015. Rupture termination at restraining bends: the last great earthquake on the Altyn Tagh fault. Geophys. Res. Lett. http://dx.doi.org/10.1002/2015GL063107 (2015GL063107).

Ferris, A., Abers, G.A., Christensen, D.H., Veenstra, E., 2003. High resolution image of the subducted Pacific (?) plate beneath central Alaska, 50–150 km depth. Earth Planet. Sci. Lett. 214, 575–588. http://dx.doi.org/10.1016/S0012-821X(03)00403-5.

Fitzgerald, P.G., Stump, E., Redfield, T.F., 1993. Late Cenozoic uplift of Denali and its relation to relative plate motion and fault morphology. Science 259, 497–499. http://dx.doi.org/10.1126/science.259.5094.497.

Fitzgerald, P.G., Sorkhabi, R.B., Redfield, T.F., Stump, E., 1995. Uplift and denudation of the central Alaska Range: a case study in the use of apatite fission track thermochronology to determine absolute uplift parameters. J. Geophys. Res. 100, 20,175–20,191.

Fitzgerald, P.G., Roeske, S.M., Benowitz, J.A., Riccio, S.J., Perry, S.E., Armstrong, P.A., 2014a. Alternating asymmetric topography of the Alaska range along the strike-slip Denali fault: Strain partitioning and lithospheric control across a terrane suture zone. Tectonics http://dx.doi.org/10.1002/2013TC003432 (2013TC003432).

Fitzgerald, P.G., Roeske, S.M., Benowitz, J.A., Riccio, S.J., Perry, S.E., Armstrong, P.A., 2014b. Alternating asymmetric topography of the Alaska Range along the strike-slip Denali Fault: strain partitioning and lithospheric control across a terrane suture zone. Tectonics http://dx.doi.org/10.1002/2013TC003432 (2013TC003432).

Freymueller, J.T., Woodard, H., Cohen, S.C., Cross, R., Elliott, J., Larsen, C.F., Hreinsdóttir, S., Zweck, C., 2008. Active Deformation Processes in Alaska, Based on 15 Years of GPS Measurements. In: Freymueller, J.T., Haeussler, P.J., Wesson, R., Ekström, G. (Eds.), Active Tectonics and Seismic Potential of Alaska, American Geophysical Union Geophysical Monograph Series. American Geophysical Union, Washington, D.C, pp. 1–42.

Gilbert, W.G., Ferrell, V.M., Turner, D.L., 1976. The Teklanika Formation: A New Paleocene Volcanic Formation in the Central Alaska Range, Geologic Report. Alaska Division of Geological & Geophysical Surveys.

Gomez, F., Nemer, T., Tabet, C., Khawlie, M., Meghraoui, M., Barazangi, M., 2007. Strain partitioning of active transpression within the Lebanese restraining bend of the Dead Sea Fault (Lebanon and SW Syria). Geol. Soc. Lond., Spec. Publ. 290, 285–303. http://dx.doi.org/10.1144/290.10.

Haeussler, P.J., 2008. An overview of the neotectonics of interior Alaska: far-field deformation from the Yakutat Microplate Collision, in: Freymueller, J.T., Haeussler, P.J., Wesson, R.L., Ekström, G. (Eds.), Active Tectonics and Seismic Potential of Alaska, American Geophysical Union Geophysical Monograph Series. American Geophysical Union, Washington, D.C, pp. 83–108.

Haeussler, P.J., Matmon, A., Schwartz, D.P., Seitz, G., Crone, A.J., 2012. The Denali fault and interior Alaska tectonics in mid- to late-Cenozoic time. Eos Transactions. Presented at the American Geophysical Union Fall Meeting, pp. T14A–T104.

Hatem, A.E., Cooke, M.L., Madden, E.H., 2015. Evolving efficiency of restraining bends within wet kaolin analog experiments. J. Geophys. Res. Solid Earth http://dx.doi.org/10.1002/2014JB011735 (2014JB011735).

Jadamec, M.A., Billen, M.I., Roeske, S.M., 2013. Three-dimensional numerical models of flat slab subduction and the Denali fault driving deformation in south-central Alaska. Earth Planet. Sci. Lett. 376, 29–42. http://dx.doi.org/10.1016/j.epsl.2013.06.009.

Koehler, R.D., Farrel, R.-E., Burns, P.A.C., Combellick, R.A., 2012. Quaternary Faults and Folds in Alaska: A Digital Database (Alaska Division of Geological & Geophysical Surveys Miscellaneous Publication No. 141.

Leever, K.A., Gabrielsen, R.H., Sokoutis, D., Willingshofer, E., 2011. The effect of convergence angle on the kinematic evolution of strain partitioning in transpressional brittle wedges: insight from analog modeling and high-resolution digital image analysis. Tectonics 30, TC2013. http://dx.doi.org/10.1029/2010TC002823.

Legg, M.R., Goldfinger, C., Kamerling, M.J., Chaytor, J.D., Einstein, D.E., 2007. Morphology, structure and evolution of California Continental Borderland restraining bends. Geol. Soc. Lond., Spec. Publ. 290, 143–168. http://dx.doi.org/10.1144/SP290.3.

Little, T.A., 1990. Kinematics of wrench and divergent-wrench deformation along a central part of the Border Ranges Fault System, Northern Chugach Mountains, Alaska. Tectonics 9, 585–611. http://dx.doi.org/10.1029/TC009i004p00585.

Lozos, J.C., Oglesby, D.D., Duan, B., Wesnousky, S.G., 2011. The effects of double fault bends on rupture propagation: a geometrical parameter study. Bull. Seismol. Soc. Am. 101, 385–398. http://dx.doi.org/10.1785/0120100029.

Mann, P., 2007. Global catalogue, classification and tectonic origins of restraining- and releasing bends on active and ancient strike-slip fault systems. Geol. Soc. Lond., Spec. Publ. 290, 13–142. http://dx.doi.org/10.1144/SP290.2.

Matmon, A., Briner, J.P., Carver, G., Bierman, P., Finkel, R.C., 2010. Moraine chronosequence of the Donnelly Dome region, Alaska. Quat. Res. 74, 63–72. http://dx.doi.org/10.1016/j.yqres.2010.04.007.

Mériaux, A.-S., Sieh, K., Finkel, R.C., Rubin, C.M., Taylor, M.H., Meltzner, A.J., Ryerson, F.J., 2009. Kinematic behavior of southern Alaska constrained by westward decreasing postglacial slip rates on the Denali Fault, Alaska. J. Geophys. Res. 114, B03404. http://dx.doi.org/10.1029/2007JB005053.

Péwé, T.L., Wahrhaftig, C., Weber, F.R., 1966. Geologic map of the Fairbanks quadrangle, Alaska (Miscellaneous Investigations No. I-455), U.S. Geological Survey Miscellaneous Investigations I-455. U.S. Geol. Surv. 1, 63,360.

Plafker, G., Berg, H.C., 1994. Overview of the geology and tectonic evolution of Alaska. In: Plafker, G., Berg, H.C. (Eds.), The Geology of Alaska G-1. Geological Society of America, Geology of North America, Boulder, Colorado, pp. 989–1021.

Plafker, G., Naeser, C.W., Zimmerman, R.A., Lull, J.S., Hudson, T., 1992. Cenozoic uplift history of the Mount McKinley area in the central Alaska Range based on fission-track dating. In: Bradley, D.C., Dusel-Bacon, C. (Eds.), 202 Geologic Studies in Alaska by the U.S. Geological Survey, 1991. U.S. Geological Survey Bulletin, pp. 202–212.

Plafker, G., Gilpin, L.M., Lahr, J.C., 1994. Neotectonic Map of Alaska, in: Plafker, G., Berg, H.C. (Eds.), The Geology of Alaska. Boulder, Colorado, Geological Society of America, Geology of North America, v. G-1, plate 12, 1:2,500,000.

Ratchkovski, N.A., Hansen, R.A., 2002. New constraints on tectonics of Interior Alaska: earthquake locations, source mechanisms, and stress regime. Bull. Seismol. Soc. Am. 92, 998–1014. http://dx.doi.org/10.1785/0120010182.

Reed, J.C., 1961. Geology of the Mount McKinley Quadrangle, Alaska (U.S. Geological Survey Bulletin No. 1108-A).

Reed, B.L., Nelson, S.W., 1980. Geologic Map of the Talkeetna Quadrangle Alaska.

Riccio, S.J., Fitzgerald, P.G., Benowitz, J.A., Roeske, S.M., 2014. The role of thrust faulting in the formation of the eastern Alaska Range: thermochronological constraints from the Susitna Glacier Thrust Fault region of the intracontinental strike-slip Denali Fault system. Tectonics 33. http://dx.doi.org/10.1002/2014TC003646 (2014TC003646).

Ridgway, K.D., Trop, J.M., Sweet, A.R., 1997. Thrust-top basin formation along a suture zone, Cantwell basin, Alaska Range: Implications for development of the Denali fault system. Geol. Soc. Am. Bull. 109, 505–523. http://dx.doi.org/10.1130/0016-7606(1997)109<0505:TTBFAA>2.3.CO;2.

Ridgway, K.D., Trop, J.M., Nokleberg, W.J., Davidson, C.M., Eastham, K.R., 2002. Mesozoic and Cenozoic tectonics of the eastern and central Alaska Range: Progressive basin development and deformation in a suture zone. Geol. Soc. Am. Bull. 114, 1480–1504. http://dx.doi.org/10.1130/0016-7606(2002)114<1480:MACTOT>2.0.CO;2.

Ridgway, K.D., Thoms, E.E., Layer, P.W., Lesh, M.E., White, J.M., Smith, S.V., 2007. Neogene transpressional foreland basin development on the north side of the central Alaska Range, Usibelli Group and Nenana Gravel, Tanana basin. In: Ridgway, K.D., Trop, J.M., Glen, J.M.G., O'Neill, J.M. (Eds.), Tectonic Growth of a Collisional Continental Margin: Crustal Evolution of Southern Alaska, Geological Society of America Special Paper, pp. 507–547.

Ruppert, N.A., Ridgway, K.D., Freymueller, J.T., Cross, R.S., Hansen, R.A., 2008. Active tectonics of Interior Alaska: seismicity, GPS geodesy, and local geomorphology. In: Freymueller, J.T., Haeussler, P.J., Wesson, R., Ekström, G. (Eds.), Active Tectonics and Seismic Potential of Alaska, Geophysical Monograph Series 179. American Geophysical Union, Washington, D.C, pp. 109–133.

Salazar-Jaramillo, S., Fowell, S.J., McCarthy, P.J., Benowitz, J.A., Śliwiński, M.G., Tomsich, C.S., 2016. Terrestrial isotopic evidence for a Middle-Maastrichtian warming event from the lower Cantwell Formation, Alaska. Palaeogeography, Palaeoclimatology, Palaeoecology, Selected Papers Based on Geological Society of America, Annual Meeting, Theme Session 241, Ancient Polar Ecosystems and Climate History in Deep Time, Denver, Colorado, USA, 30 October 2013. 441, Part 2, pp. 360–376. http://dx.doi.org/10.1016/j.palaeo.2015.09.044.

Schwartz, D.P., Coppersmith, K.J., 1984. Fault behavior and characteristic earthquakes: examples from the Wasatch and San Andreas fault zones. J. Geophys. Res. 89, 5681–5698.

Schwartz, D.P., Coppersmith, K.J., 1986. Seismic hazards: new trends in analysis using geologic data. Active Tectonics, Studies in Geophysics. National Research Council, p. 266.

Fault segmentation and controls of rupture initiation and termination. In: Schwartz, D.P., Sibson, R.H. (Eds.), U.S. Geological Survey Open-file Report 89-315.

Ten Brink, N.W., Waythomas, C.F., 1985. Late Wisconsin glacial chronology of the North-Central Alaska Range: a regional synthesis and its implications for early human settlements (Research Report No. 19). Natl. Geogr.

Terhune, P., Benowitz, J.A., Bemis, S.P., Cooke, M.L., O'Sullivan, P.B., Burkett, C., Hatem, A., 2014. Extreme topographic development along the Denali fault strike-slip system, Alaska: why is Mount McKinley so big? Abstracts with Programs. Presented at the Geological Society of America Annual Meeting, Vancouver, BC, p. 212

Terhune, P., Benowitz, J.A., Waldien, T.S., Allen, W.K., Davis, K.N., Ridgway, K.D., Roeske, S.M., Fitzgerald, P.G., Brueseke, M.E., O'Sullivan, P.B., 2015. Geochronological framework for the Cenozoic history of the southern Alaska Range fold and thrust belt. Abstracts with Programs. Presented at the Geological Society of America Cordilleran Section Meeting, Anchorage, Alaska.

Tomsich, C.S., McCarthy, P.J., Fiorillo, A.R., Stone, D.B., Benowitz, J.A., O'Sullivan, P.B., 2014. New zircon U–Pb ages for the Lower Cantwell Formation: implications for Late Cretaceous paleoecology and paleoenvironment at Sable Mountain, Denali National Park, Alaska. ICAM VI Proceedings, pp. 19–60.

Trop, J.M., Ridgway, K.D., 2007. Mesozoic and Cenozoic tectonic growth of southern Alaska: a sedimentary basin perspective. Special Paper 431: Tectonic Growth of a Collisional Continental Margin: Crustal Evolution of Southern Alaska 431 pp. 55–94. http://dx.doi.org/10.1130/2007.2431(04).

Wahrhaftig, C., 1958. Quaternary geology of the Nenana River valley and adjacent part of the Alaska Range. In: Wahrhaftig, C., Black, R.F. (Eds.), Quaternary and Engineering Geology in the Central Part of the Alaska Range, U.S. Geological Survey Professional Paper, pp. 1–73.

Wahrhaftig, C., 1987. The Cenozoic section at Suntrana, Alaska. Centennial Field Guide Volume 1: Cordilleran section of the Geological Society of America. America 1, 445–450. http://dx.doi.org/10.1130/0-8137-5401-1.445.

Wakabayashi, J., 2007. Stepovers that migrate with respect to affected deposits: field characteristics and speculation on some details of their evolution. Geol. Soc. Lond., Spec. Publ. 290, 169–188. http://dx.doi.org/10.1144/SP290.4.

Wesnousky, S.G., 2006. Predicting the endpoints of earthquake ruptures. Nature 444, 358–360. http://dx.doi.org/10.1038/nature05275.

Wilson, F.H., Dover, J.H., Bradley, D.C., Weber, F.R., Bundtzen, T.K., Haeussler, P.J., 1998. Geologic Map of Central (interior) Alaska (Open-file Report No. 98-133-A). U.S. Geological Survey.

Worthington, L.L., Van Avendonk, H.J.A., Gulick, S.P.S., Christeson, G.L., Pavlis, T.L., 2012. Crustal structure of the Yakutat terrane and the evolution of subduction and collision in southern Alaska. J. Geophys. Res. 117, B01102. http://dx.doi.org/10.1029/2011JB008493.

Yıkılmaz, M.B., Turcotte, D.L., Heien, E.M., Kellogg, L.H., Rundle, J.B., 2014. Critical jump distance for propagating earthquake ruptures across step-overs. Pure Appl. Geophys. 1–7 http://dx.doi.org/10.1007/s00024-014-0786-y.